Satellite-derived Constraints on the Effect of Drought Stress on Biogenic Isoprene Emissions in the Southeast US

Yuxuan Wang[1], Nan Lin[1], Wei Li[1], Alex Guenther[2], Joey C. Y. Lam[3], and Amos P. K. Tai[3,4], Mark J. Potosnak[5], Roger Seco[6]

[1] Department of Earth and Atmospheric Sciences, University of Houston, Houston, Texas, USA.

[2] Earth System Science, University of California, Irvine, Irvine, California, USA

[3] Earth and Environmental Sciences Programme, Faculty of Science, The Chinese University of Hong Kong, Hong Kong SAR, China

[4] State Key Laboratory of Agrobiotechnology and Institute of Environment, Energy and Sustainability, The Chinese University of Hong Kong, Hong Kong SAR, China

[5] Environmental Science and Studies, DePaul University, Chicago, IL, USA

[6] Institute of Environmental Assessment and Water Research (IDAEA-CSIC), Carrer Jordi Girona 18-26, 08034 Barcelona, Spain

Corresponding author: Yuxuan Wang (ywang246@central.uh.edu)

Abstract. While substantial progress has been made to improve our understanding of biogenic isoprene emissions under unstressed conditions, there remain large uncertainties in isoprene emissions under stressed conditions. Here we use the US Drought Monitor (USDM) as a weekly drought severity index and tropospheric columns of formaldehyde (HCHO), the key product of isoprene oxidation, retrieved from the Ozone Monitoring Instrument (OMI) to derive top-down constraints on the response of summertime isoprene emissions to drought stress in the Southeast U.S. (SE US), a region of high isoprene emissions and prone to drought. OMI HCHO column density is found to be 6.7% (mild drought) - 23.3% (severe drought) higher than that in no-drought conditions. A global chemical transport model, GEOS-Chem, with the MEGAN2.1 emission algorithm can simulate this direction of change, but the simulated increases at the corresponding drought levels are 1.1-1.5 times of OMI HCHO, suggesting the need for a drought-stress algorithm in the model. By minimizing the model-to-OMI differences in HCHO to temperature sensitivity under different drought levels, we derived a top-down drought stress factor (γ_{d_OMI}) in GEOS-Chem that parameterizes using water stress and temperature. The algorithm led to an 8.6% (mild drought) - 20.7% (severe drought) reduction in isoprene emissions in the SE US relative to the simulation without it. With γ_{d_OMI} the model predicts a non-linear increasing trend in isoprene emissions with drought severity that is consistent with OMI HCHO and a single site's isoprene flux measurements. Compared with a previous drought stress algorithm derived from the latter, the satellite-based drought stress factor performs better in capturing the regional scale drought-isoprene responses as indicated by the close-to-zero mean bias between OMI and simulated HCHO columns under different drought conditions. The drought stress algorithm also reduces the model's high bias in organic aerosols (OA) simulations by 6.60% (mild drought) to 11.71% (severe drought) over the SE US compared to the no-stress simulation. The simulated ozone response to the drought stress factor displays a spatial disparity due to the isoprene suppressing effect on oxidants, with an <1 ppb increase in O_3 in high-isoprene regions and a 1-3 ppbv decrease in O_3 in low-isoprene regions. This

study demonstrates the unique value of exploiting long-term satellite observations to develop empirical stress
algorithms on biogenic emissions where in situ flux measurements are limited.

1. Introduction

Biogenic nonmethane volatile organic compounds (BVOCs) emitted by terrestrial ecosystems are of great importance to air quality, tropospheric chemistry, and climate due to their effects on atmospheric oxidants and aerosols (Atkinson, 2000; Claeys et al., 2004; Pacifico et al., 2009). The dominant BVOC is isoprene ($CH_2=C(CH3)CH=CH_2$), comprising 70% of the global total BVOC emitted from vegetation (Sindelarova et al., 2014). Isoprene emissions depend on vegetation/plant type, physiological status, leaf age, and meteorological conditions such as radiation, temperature, and soil moisture. These relationships provide the basic framework of isoprene emission models that are capable of coupling with meteorology and the land biosphere, the most widely used being the Model of Emissions of Gases and Aerosols from Nature (MEGAN) (Guenther et al., 1993, 2006, 2012, 2017). Recent work has shown stressed conditions - such as drought, heatwaves, and high winds - can induce large changes in isoprene emissions different from model predictions in the absence of those stress factors (Potosnak et al., 2014; Huang et al., 2015; Kravitz et al., 2016; Seco et al., 2015; Otu-Larbi et al., 2020; Seco et al., 2022). As stressed conditions are rarely sampled by field campaigns due to their infrequent and irregular nature and hence poorly constrained, stress impacts on isoprene emissions are among the least understood aspects in our predictivity of BVOC-chemistry-climate interactions.

A common stress for terrestrial vegetation worldwide is drought, characterized by low precipitation, high temperature, and low soil moisture (Trenberth et al., 2014). These conditions are primary abiotic stresses that will cause physiological impacts on plants affecting photosynthesis, stomatal conductance, transpiration, and leaf area. During short-term or mild droughts, the photosynthetic rate of plants quickly decreases due to limited stomatal conductance, while isoprene is not immediately impacted because of the availability of stored carbon and because the photosynthetic electron transport is not inhibited. Isoprene can even increase by several factors due to warm leaf temperatures which increases isoprene synthase activity (Potosnak et al., 2014; Ferracci et al., 2020). During prolonged or severe drought stress, after a lag related to photosynthesis reduction, isoprene emission eventually declines because of inadequate carbon availability. This conceptualized non-monotonic response of isoprene emission to drought has been demonstrated at the Missouri Ozarks AmeriFlux (MOFLUX) field site in Missouri (Potosnak et al., 2014; Seco et al., 2015), the only available drought-relevant whole canopy isoprene flux measurements to date, and qualitatively supported by ambient isoprene concentrations monitored by regional surface networks (Wang et al., 2017). It is noteworthy that the MOFLUX data covered only two drought events (summer 2011 and summer 2012), while the surface sites are sparsely distributed with an urban focus. More recently, the isoprene concentration measurements during the Wytham Isoprene iDirac Oak Tree Measurements (WIsDOM) campaign showed that isoprene was up to four times higher than normal in responses to a combined heatwave and drought episode (June-October 2018) over a mid-latitude temperate forest in the UK (Ferracci et al., 2020; Otu-Larbi et al., 2020), which supports the enhanced isoprene emissions at the MOFLUX site under mild droughts. However, these observations offer only limited constraints on drought stress impacts on isoprene emissions.

With wide spatiotemporal coverage, satellite provides arguably the best platform to capture drought development and impacts. Satellite observations of tropospheric formaldehyde (HCHO) columns have been used as a proxy of isoprene emissions for more than a decade (Abbot et al., 2003; Palmer et al., 2003), as HCHO is formed promptly and in high yield from isoprene oxidation (Sprengnether et al., 2002). Previous applications of satellite HCHO products provided "top-down" estimates on seasonality, magnitude, spatial distribution, and interannual variability of isoprene emissions globally and regionally (e.g., Marais et al., 2016; Kaiser et al., 2018; Stavrakou et al., 2018). While most of these studies focused on *unstressed* conditions, recent efforts have shown that satellite HCHO registered drought signals on a monthly scale (Zheng et al., 2017; Naimark et al., 2021; Li et al., 2022; Opacka et al., 2022). These signals are yet to be exploited to constrain isoprene response to drought.

The present study aims at improving the current quantification of satellite HCHO response to drought by accounting for sub-monthly variability of drought severity. We use a weekly time scale, the finest temporal scale of drought indices available, and separate five levels of drought severity defined by the US Drought Monitor. By comparison, previous investigations used binary classification (drought or not) on a monthly time scale. Our improvement in scale is expected to better capture the nonlinear response of isoprene emissions to drought severity as described above. The study region is the Southeast United States (SE US), which has large isoprene emissions due to substantial forest coverage and is also prone to drought due to large interannual variability in precipitation (Seager et al., 2009). In addition, the MOFLUX site is located in the SE US, which will allow us to evaluate if satellite-derived drought responses of HCHO are consistent with those from isoprene flux measurements at MOFLUX. Finally, we use these HCHO signals in conjunction with models to identify the model gaps in predicting isoprene responses to drought.

2. Data and Method

2.1 Drought index

There are many types of drought indices focusing on different factors, including precipitation, temperature, evaporation, runoff, and the impact of drought on ecosystems and vegetation (Palmer, 1965; McKee et al., 1993; Guttman, 1999; Vicente-Serrano et al., 2010; Chang et al., 2018). Drought indices also differ by time scale. As drought by definition is a prolonged period of water deficit, the shortest time scale of drought is weekly. Here we chose the United States Drought Monitor (USDM) drought index to identify drought periods. USDM's weekly timescale and multiple drought severity levels (Svoboda et al., 2002) provide a better delineation of drought variability than the monthly or seasonal scale used in the previous analysis of drought signals in HCHO and isoprene (Wang et al., 2017; Naimark et al., 2021).

(a) USDM released on July 12,2012   (b) USDM time series for SE US

☐ N0 Wet and Normal   ◼ D0 Abnormal Drought   ◼ D1 Moderate Drought
◼ D2 Severe Drought   ◼ D3 Extreme Drought   ◼ D4 Exceptional Drought
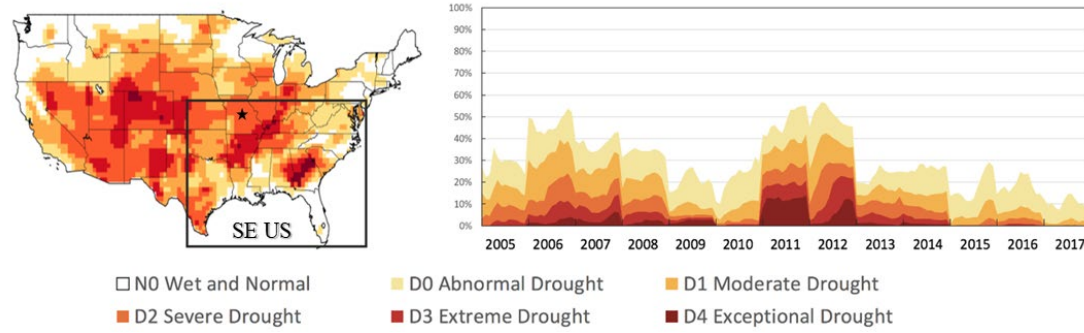
Figure 1. (a) Drought distribution for the second week of July 2012 based on USDM. The black star indicates the location of MOFLUX site. (b) Time series of drought frequency in the study area (black box in Figure 1a) for JJA from 2005 to 2017. N0 (white) for wet and normal, D0 (light yellow) for abnormal drought, D1 (yellow) for moderate drought, D2 (orange) for severe drought, D3 (red) for extreme drought, and D4 (brown) for exceptional drought.

The USDM is a composite drought index based on six key physical indicators including the Palmer Drought Severity Index (PDSI, Palmer, 1965), CPC Soil Moisture Model Percentiles (Huang et al., 1996), U.S. Geological Survey (USGS) Daily Streamflow Percentiles (http://water.usgs.gov.waterwatch/), Percent of Normal Precipitation (Willeke et al., 1994), Standardized Precipitation Index (SPI, McKee et al., 1993), and remotely sensed Satellite Vegetation Health Index (Kogan, 1995). Opinions of local experts are also considered (Svoboda et al., 2002). The USDM website (https://droughtmonitor.unl.edu/) provides weekly ArcGIS shapefiles of the polygons covering the whole US under five drought levels: D0 for abnormal drought, D1 for moderate drought, D2 for severe drought, D3 for extreme drought, and D4 for exceptional drought. We used the method of Chen et al. (2019) to rasterize and convert USDM shapefiles to $0.5° \times 0.5°$ gridded indices with -1 indicating non-drought (N0) and 0-4 for D0-D4 drought, respectively. **Figure 1a** displays the spatial distribution of gridded USDM indices for the second week of July 2012, which clearly depicts the extent and severity of the infamous 2012 Great Plains drought (Hoerling et al., 2014). **Figure 1b** shows the weekly time series of USDM indices averaged over SE US (75–100◦W, 25–40◦N, black box in Figure 1a) for the summer months (June, July, August; JJA) of 2005 -2017, our study period. During this period, abnormal drought (D0) appeared every summer, while extreme and exceptional drought (D3-D4) were mainly concentrated in 2006-2008 and 2010-2012. This pattern is consistent with the long-term drought statistics from other drought indices such as SPEI and PDSI (Svoboda et al., 2015).

2.2 OMI HCHO and NO₂ product

We used the Ozone Monitoring Instrument (OMI) v003 level 3 tropospheric formaldehyde (HCHO) column density (OMHCHOd) as described by Chance (2019). OMI was launched on NASA's Aura satellite in 2004 and has since provided daily global measurements of ozone (O_3) and its precursors with a nadir spatial resolution of 24×13 km^2. Since January 2009, OMI has been suffering from a major row anomaly. OMHCHOd data processing explored all level 2 OMHCHO observations to filter out pixels with bad formaldehyde retrievals, high cloud fractions (>30%), high SZA (>70°), and pixels affected by OMI's row anomaly (Chance, 2019). The spatial resolution is $0.1° \times 0.1°$. Zhu et al. (2016) verified the OMHCHOd data using high-precision HCHO aircraft observations obtained during

129   NASA SEAC4RS activities in SE US from August to September 2013. They showed that OMI retrievals have accurate

130   spatial and temporal distribution but were biased low by 37% relative to the aircraft. We corrected this underestimation

131   by applying a uniform and constant factor of 1.5 to the OMHCHOd data, as did by Shen et al. (2019) in their long-

132   term analysis of OMI HCHO. **Figure 2a** presents the corrected OMHCHOd for the SE US averaged over JJA 2005-

133   2017, where higher levels of HCHO are clearly seen over forested regions in Missouri, Georgia, Arkansas, and Texas.

134   OMHCHOd values shown hereafter are those with the correction factor applied. Although it is not known if the

135   correction factor has temporal spatial variations during our study period, its application produced a good match

136   between OMI and simulated HCHO columns under non-drought (N0) conditions (Figure 2c). To examine the

137   concurrent changes of nitrogen oxides ($NO_x = NO_2 + NO$) under droughts, we also used the level 3 tropospheric

138   column of NO_2 from OMI during the same period.

139
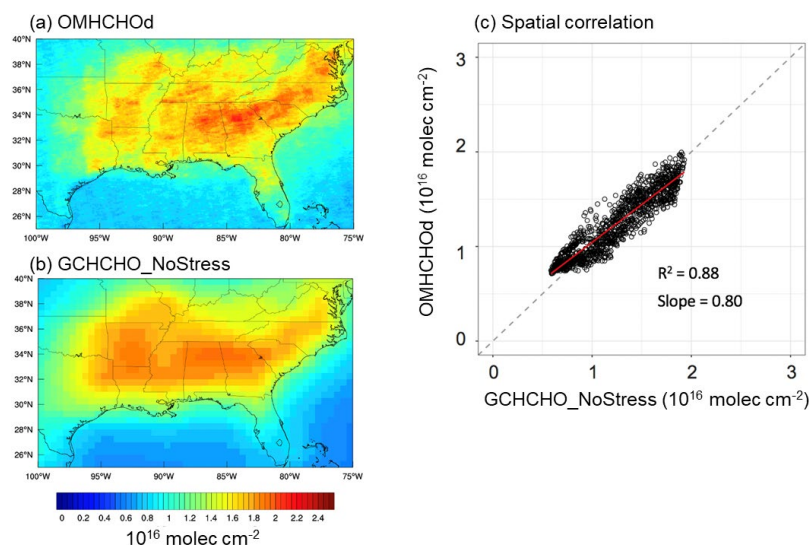
140   **Figure 2. Mean 2005–2017 HCHO columns for June – August over the SE US of (a) OMI observation (OMHCHOd) and**
141   **(b) GEOS-Chem simulation (GCHCHO_NoStress). (c) Scatterplot of spatial correlation between the two. The dashed line**
142   **indicates the 1:1 agreement.**

143   **2.3 GEOS-Chem chemical transport model**

144   We used the long-term simulation of the nested-grid GEOS-Chem global chemical transport model (version 12-02,

145   http://www.geos-chem.org) to obtain daily mean results of modeled formaldehyde columns and isoprene emissions

146   for North America during JJA 2005 – 2017. The simulation was driven by the Modern-Era Retrospective analysis for

147   Research and Applications, Version 2 (MERRA-2) meteorological data from NASA's Global Modeling and

148   Assimilation Office (GMAO) with a horizontal resolution at $0.5° × 0.625°$. Biogenic emissions were calculated using

149   MEGAN2.1, which is the prevailing version of MEGAN implemented in most chemical and climate models.

150   MEGAN2.1 has a soil dependence algorithm whose parameterization is based on plant wilting point threshold and

151   soil moisture (Guenther et al., 2017). However, this factor is disabled in GEOS-Chem as in many other CTMs due to

152   the unavailability of the required driving variables, such as wilting point and soil moisture, which cannot be simulated

153   well in most models (Trugman et al., 2018). Thus, outputs from the standard GEOS-Chem simulations do not have

154 drought effects on isoprene emissions and these outputs are referred to as NoStress_GC. Anthropogenic emissions
155 over North America were from the 2011 National Emissions Inventory (NEI2011, http://www.epa.gov/air-emissions-
156 inventories) for the United States, with historical scale factors applied to each simulated year. Open fire emissions
157 were from GFED4 (Giglio et al., 2013) for 2005–2017.

158 To better match with OMI overpassing time, model HCHO outputs at 13:30 local time were sampled
159 (GCHCHO_NoStress). **Figure 2b** shows GCHCHO_NoStress averaged over the same domain and period as
160 OMHCHOd in **Figure 2a**. The scatter plot (**Figure 2c**) shows a good spatial correlation between the two ($R^2 = 0.88$).
161 This correlation is consistent with other studies comparing GEOS-Chem and OMI HCHO columns in SE US during
162 non-drought periods (Kaiser et al., 2018).

163 **2.4 Observations of ozone, organic aerosol, LAI, and isoprene flux**

164 To evaluate how the drought stress factor changes the simulations of surface O_3 and organic aerosol (OA), we adopted
165 the gridded ($1° \times 1°$) hourly O_3 observations created by Schnell et al. (2014) using the modified inverse distance
166 weighting method. The dataset aggregates several networks of O_3 measurements including the US Environmental
167 Protection Agency's (EPA) Air Quality System (AQS), Clean Air Status and Trends Network (CASTNET), and
168 Environment Canada's National Air Pollution Surveillance Program (NAPS). Following the same method, we created
169 a gridded organic aerosol (OA) dataset using the organic carbon (OC) observations from the Interagency Monitoring
170 of Protected Visual Environments (IMPROVE) network. A factor of 2.1 was used to convert OC to OA as suggested
171 by other studies (Pye et al., 2017; Schroder et al., 2018). To examine the changes of leaf area index (LAI) under
172 droughts, the MODerate resolution Imaging Spectroradiometer (MODIS) Collection 5 LAI products reprocessed by
173 Yuan et al. (2011) with a resolution of $0.25° \times 0.25°$ was used. These three datasets were further remapped through
174 bilinear interpolation to match the spatial resolution of the USDM. The isoprene flux measurements at the MOFLUX
175 site during 2012 May-September were used to derive a site-based drought stress algorithm. The site is located in the
176 Ozarks region of central Missouri (38.74°N, 92.20°W, black star in Figure 1a). It is surrounded by a deciduous forest
177 dominated by isoprene-emitting white and red oak species. The dataset is widely used to investigate isoprene emissions
178 response to droughts (Potosnak et al., 2014; Seco et al., 2015; Jiang et al., 2018; Opacka et al., 2022).

179 **3. Observational Evidence of Drought Stress on Isoprene Emissions**

180 **3.1 Changes of HCHO column densities with drought**

181 To reveal drought responses of HCHO, we sampled weekly-mean HCHO columns onto the gridded spatial and
182 temporal locations of each USDM category and generated average HCHO distributions at each drought level over the
183 SE US. The outputs are shown in **Figure 3a** for OMI and **3b** for NoStress_GC, respectively. The processing of weekly-
184 mean HCHO data corresponds to the timing of USDM: a whole week includes Wednesday of the previous week to
185 Tuesday of the present week. There are 12 consecutive weeks from June to August in each year of 2005-2017, giving
186 a total of 156 weeks' gridded HCHO data to be assigned to individual USDM categories by week and location. **Figure**
187 **3d** shows the number of weeks underlying the gridded averages of HCHO for each USDM category. As severe

188   droughts are less frequent than mild droughts, some locations in SE US did not experience D2-D4 droughts during the

189   study period and hence are shown as white in **Figure 3**.

190   10^{16} molec cm^{-2} 10^{16} molec cm^{-2} 10^{-10} kg m^{-2} s^{-1}
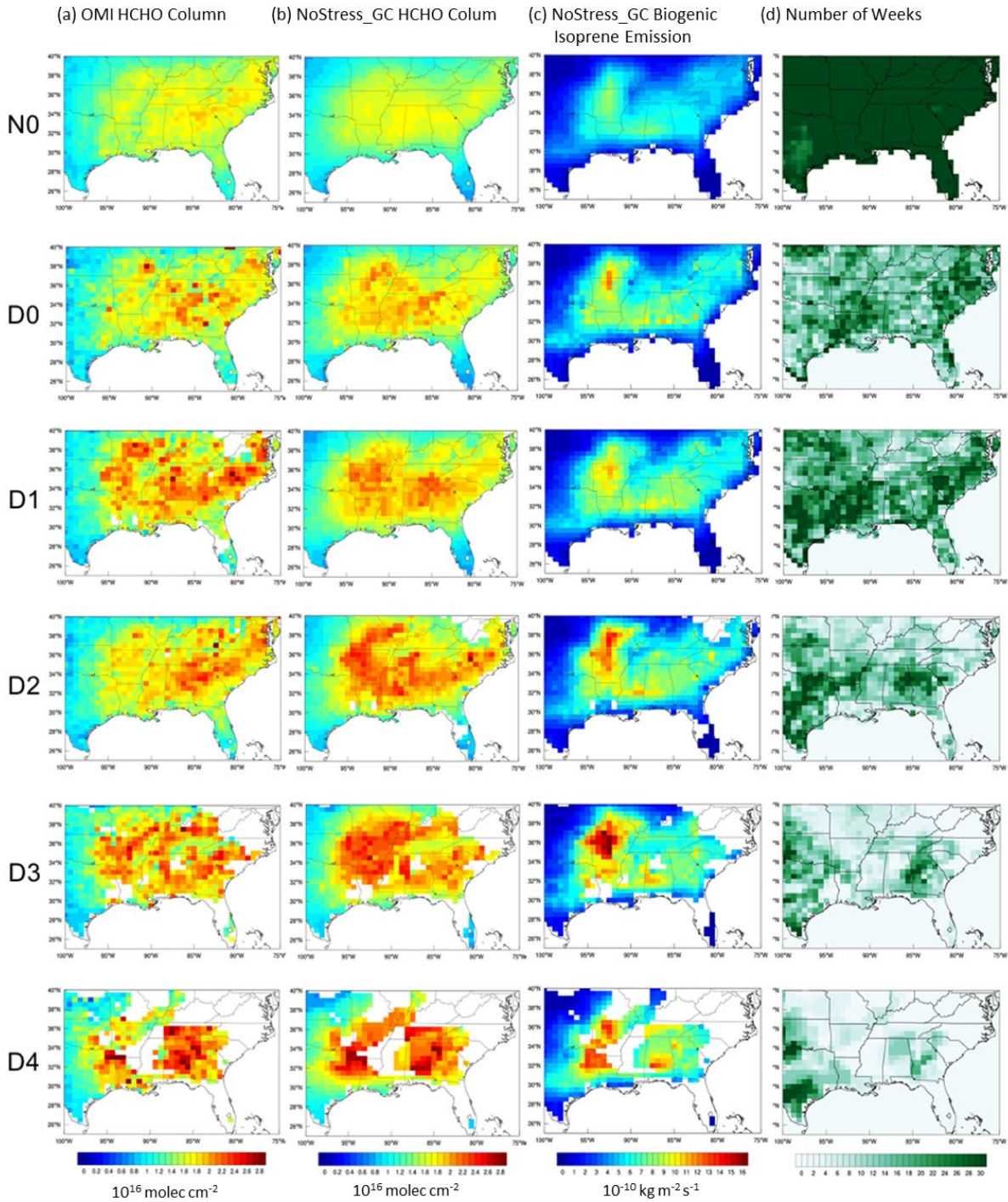
191   **Figure 3. The mean spatial distributions of (a) OMI HCHO column density; (b) NoStress_GC HCHO column density, (c)**
192   **NoStress_GC isoprene emissions, and (d) the number of weeks during JJA 2005 to 2017 in the southeast US under different**
193   **USDM drought levels (N0, D0-D4).**

194   OMI HCHO column density increases with increasing drought severity in almost all locations in the SE US (**Figure**
195   **3a**). Relative to no-drought condition (N0), the mean HCHO column from OMI is 6.7%, 12.6%, 16.5%, 21.2%, and
196   23.2% higher under D0 - D4 drought in the entire SE US, respectively. These HCHO changes are statistically
197   significant at a 95% confident interval, indicating that the OMI HCHO products contain significant drought signals.
198   The increasing rate of OMI HCHO with USDM is not linear, faster under mild droughts (D0-D2) and flattening under
199   more severe droughts (D2-D4). This is qualitatively consistent with the conceptualized model of the nonlinear
200   response of isoprene emissions to drought described before (Potosnak et al., 2014).

201   Model HCHO column density also increases with increasing drought severity (**Figure 3b**). GCHCHO_NoStress is
202   9.90%, 15.1%, 19.5%, 21.8%, and 29.1% higher under D0-D4 drought than that of N0, respectively. These increases
203   are 1.1-1.5 times those of OMI under all drought levels. The model comparison against OMI HCHO also changes
204   with drought severity. GCHCHO_NoStress has a minimal bias (0.05×10^{16} molec cm^{-2}) under N0. As drought severity
205   increases, the mean bias over the entire SE US increases to 0.10×10^{16} molec cm^{-2}, 0.09×10^{16} molec cm^{-2}, $0.11 \times$
206   10^{16} molec cm^{-2}, 0.08×10^{16} molec cm^{-2}, and 0.15×10^{16} molec cm^{-2} under D0 - D4 levels, respectively. The spatial
207   correlation between OMI and NoStress_GC degrades with USDM, with R^2 being smaller than 0.65 under D0 - D4
208   levels compared to R^2 of 0.70 under N0. Worsening model performance with increasing drought severity suggests the
209   model lacks a process that changes with drought. As isoprene accounts for more than 80% of the contribution of non-
210   methane VOCs to the HCHO column in the southeast US(Palmer et al., 2003; Millet et al., 2006), the missing process
211   is most likely drought-induced changes in isoprene emissions.

212
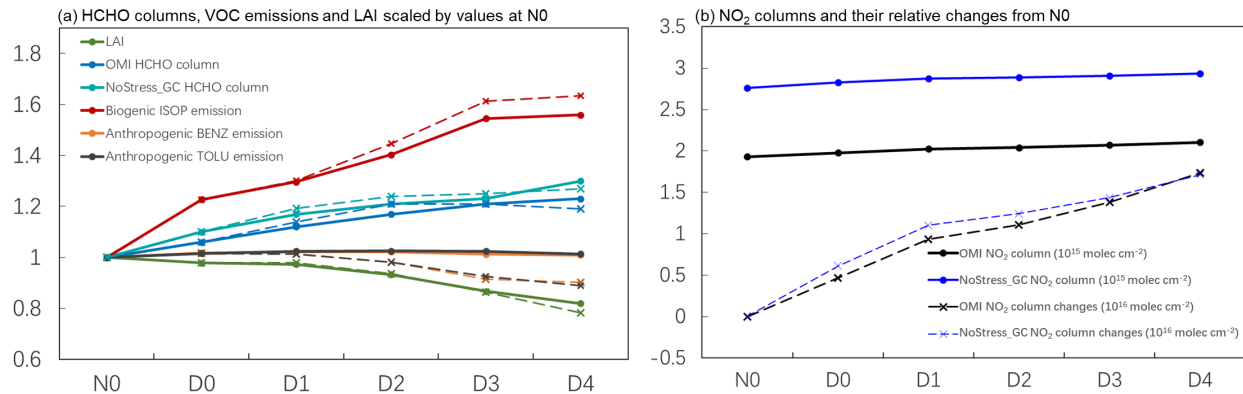
213   **Figure 4. (a) Relative changes of regional-mean OMI HCHO column, NoStress_GC simulated HCHO colum, isoprene**
214   **emissions, anthropogenic benzene emission, anthropogenic toluene emission, and MODIS leaf area index (LAI) under**
215   **different drought levels in the southeast US. All data are scaled to their respective values at N0. The dotted lines are the**
216   **arithmetic mean of all grids, and the solid lines are the corrected mean excluding the missing area. (b) Regional-mean**
217   **tropospheric NO₂ columns from OMI and NoStress_GC (solid lines), and their respective changes from non-drought (N0)**
218   **conditions (dashed lines). Note the different scales between the solid and dashed lines. The calculation is based on the grids**
219   **with the presence of all USDM levels.**

220   **Figure 4a** displays the relative changes in the regional mean HCHO column from OMI and NoStress_GC, emissions
221   of isoprene and select anthropogenic VOCs from NoStress_GC, and MODIS LAI as a function of USDM indices,
222   each scaled by its respective value at N0. The dotted line is the arithmetic mean of all available grids under each
223   dryness category, and the solid line is the mean for those grids with valid data in all dryness categories (i.e., removing

white areas shown in Figure 3). In either calculation, NoStress_GC overestimates the relative increase of HCHO under D0-D4 by 10-50% compared to OMI. After correcting for no data areas at D2-D4, isoprene emissions in NoStress_GC are 22.7%, 29.6%, 40.3%, 54.5%, and 56.0% higher in D0-D4 than N0. Note that LAI is observed to decrease by 5-10% per USDM level (**Figure 4a**), which makes the predicted increase of isoprene emissions with drought severity even more remarkable. This is likely caused by the increasingly higher temperature under droughts, given the exponential relationship of isoprene emissions with temperatures in MEGAN (Guenther et al., 2006).

By comparison, the modeled increase of the HCHO column with drought is 12-25%, more buffered than that of isoprene emissions. This is mainly caused by the loss of HCHO to photolysis, which is expected to increase under droughts with clearer skies. In addition, HCHO formation also depends on the abundance of oxidants, such as hydroxyl radicals (OH) and NO_x, that oxidize isoprene. High isoprene emissions can suppress OH under the low-NO_x conditions that prevail in part of the SE US (Wells et al., 2020), leading to the buffered response in HCHO. Previous studies (Travis et al., 2016; Kaiser et al., 2018) showed that the NEI2011 anthropogenic inventory in the model were biased high in the SE US and a reduction of 60% of NO_x emission was suggested. By comparing to OMI NO_2 column, we found NoStress_GC indeed overestimates NO_2 columns by ~42% in the SE US (**Figure 4b**), but the absolute bias in NO_2 is nearly constant from N0 to D4 (solid lines in Figure 4b). NO_2 column also shows an increasing trend from N0 to D4, yet with a much smaller rate (less than 9%) than HCHO. The model captures the relative change in NO_2 column with USDM (dashed lines in Figure 4b), despite the high bias due to the NEI2011 inventory, which indicates that the changes in natural sources of NO_x (e.g., biomass burning and soil NO_x) with droughts are well represented by NoStress_GC. To further examine the effect of high bias of NOx on simulated HCHO, we conducted a sensitivity simulation of reducing the NEI2011 NO_x emissions by 50% over the SE US during JJA 2011-2013. Most of the SE US was under droughts during the summertime of 2011-2012, while 2013 was a less drought-stricken year (**Figure 1**). The sensitivity simulation resulted in a small reduction of the simulated HCHO column and the change was nearly constant among the USDM levels (**Figure S1a-b**), ranging from -0.04×10^{16} molec cm^{-2} (2.6%) to -0.05×10^{16} molec cm^{-2} (3.5%). This rules out the possibility that the high NO_x bias in the model is the reason for the overestimation of HCHO under droughts. Given the suppression effect of isoprene on OH and the well-captured NO_2 relative changes under droughts, the overestimation of HCHO columns by the model is unlikely to be caused by model chemistry, and more likely by the overestimation of isoprene emissions under drought conditions.

While oxidation of anthropogenic VOCs also produces HCHO, using benzene and toluene as indicator species, we found no change in anthropogenic VOC emissions with drought in the model (**Figure 4a**). This insensitivity rules out anthropogenic VOCs as a key driver of model overestimation of HCHO under drought conditions. If anything, we expect anthropogenic VOC emissions to increase during drought due to higher evaporative emissions driven by higher temperature and more fossil fuel consumption driven by more demand for space cooling. Wildfires are another important source that can lead to high HCHO levels, but their contributions to HCHO are more likely to be underpredicted in GEOS-Chem partly due to insufficient hydrocarbon emissions and the underrepresented fire plume chemistry (Alvarado et al., 2020; Liao et al., 2021; Zhao et al., 2022). A deeper planetary boundary layer (PBL) is expected under droughts primarily caused by a larger sensible height flux released from dry soil (Miralles et al., 2014).

260   Indeed, the MERRA-2 PBL height used in our simulation increases by 12.42%, 17.79%, 20.99%, 26.21%, and 29.52%

261   from D0 to D4 relative to the value of 1589 m at N0 in the SE US during the midday (13:30 LT). Considering the

262   PBL heights in MERRA-2 agree well with observations with only an overall 200 m low bias (Guo et al., 2021), we

263   do not expect mixing heights to be the main cause of the high bias of HCHO column under drought conditions. To

264   further quantify the effects of wildfires and PBL on the changes of HCHO column with drought, we conducted two

265   additional sensitivity tests: (1) turning off the GFED4 wildfire emission inventory during 2011-2013 JJA, and (2)

266   keeping PBL constant as in 2013 (normal year) during 2011-2012 (drought years) JJA. The results in **Figure S1c-d**

267   show overall negligible changes in HCHO column in the SE US, which verifies our assumptions above.

268   In summary, the model overestimates HCHO increases during drought as compared to OMI. This overestimation is

269   attributed to the model overestimation of isoprene emissions during drought. Drought stress effect on isoprene

270   emissions is thus required in GEOS-Chem to resolve the discrepancy in HCHO responses to drought between OMI

271   and the model.

272   **3.2 Isoprene flux measurement**

273   To further evaluate isoprene emissions in NoStress_GC, we compared the isoprene flux measurements at the

274   MOFLUX site (Potosnak et al., 2014; Seco et al., 2015) with predicted isoprene emissions at the model grid that

275   contains the site. At the time of writing, the MOFLUX site is the only long-term, canopy-level, biogenic isoprene flux

276   measurement site in the Northern midlatitude that sampled droughts. The site experienced multiple drought levels in

277   the summer of 2012, which allows for the model-observation comparison across different drought severities as shown

278   in **Figure 5**. The abnormal dry conditions (D0) started in early June, which developed to moderate drought (D1) in

279   late June, worsened to severe drought (D2) and extreme drought (D3) in July-August, and bounced back to D2 in

280   September (**Figure 5a**). The model generally captures the daily variability of isoprene emissions with a statistically

281   significant correlation coefficient (R) of 0.67, but its biases differ by USDM levels. The model underestimates isoprene

282   flux from N0 (bias of -1.81 mg/m^2/hr) to D1 (bias of -2.89 mg/m^2/hr), has a minimal bias (-0.47 mg/m^2/hr) at D2, and

283   changes to an overestimate at D3 (bias of 1.2 mg/m^2/hr) (**Figure 5b**). While differences are expected when comparing

284   a single-point flux measurement with the grid-mean model prediction, such differences most likely result in a

285   systematic bias that should not relate to the temporal variability of drought. The fact that the model bias changes from

286   being underpredicting to overpredicting as drought severity increases further confirms the importance of the model

287   lack of a drought suppression effect on isoprene emissions during severe to exceptional droughts (D3 and D4). This

288   is qualitatively consistent with that of the HCHO biases described above.
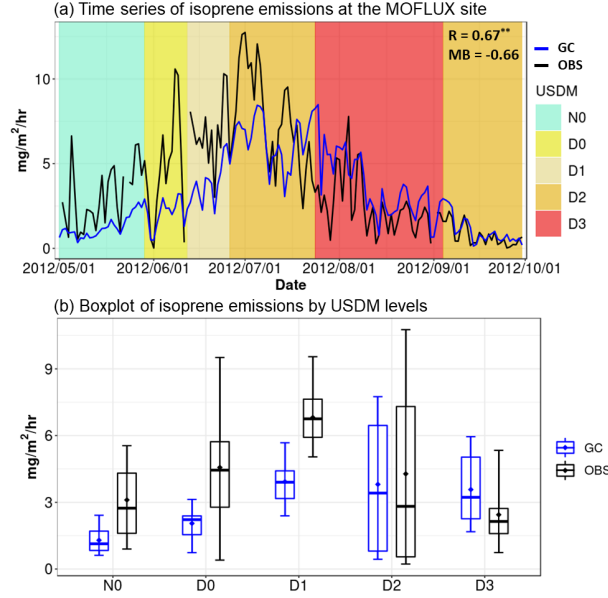
Figure 5. (a) Comparison of daily time series of isoprene emissions observed at the MOFLUX site (OBS) and simulated by MEGAN2.1 in GEOS-Chem (GC). The background is color-coded according to the USDM drought severity. R and MB at the upright corner show the correlation coefficient and mean bias, respectively. **(b)** Boxplot of isoprene emissions separated by USDM drought levels. The upper and lower whiskers represent the 90% and 10% quantiles, respectively.

4. Drought Stress Algorithm

The MEGAN2.1 isoprene emission routines in GEOS-Chem use a simplified mechanistic representation of the major environmental factors controlling biogenic emissions (Guenther et al., 2012), in which the isoprene emission factor $\gamma_{2.1}$ is the product of a canopy-related normalization factor (C_{FAC}) multiplied by other factors representing light (γ_{PAR}), temperature (γ_T), leaf age (γ_{AGE}), LAI (γ_{LAI}), carbon dioxide (CO_2) inhibition (γ_{CO2}), and soil moisture (γ_{SM}):

$$\gamma_{2.1} = C_{FAC}\gamma_{PAR}\gamma_T\gamma_{AGE}\gamma_{LAI}\gamma_{CO2}\gamma_{SM} = \gamma_0\gamma_{SM} \tag{1}$$

where γ_0 is the product of the non-drought factors. Because of the lack of reliable soil moisture databases, γ_{SM} is always set to be one in GEOS-Chem as in many other chemical transport models, which means no water stress term in the standard model configuration (i.e., NoStress_GC). We show above that NoStress_GC overestimates isoprene emissions and consequently HCHO column densities under drought conditions in the SE US. In this section, we describe the approach whereby observational constraints from the MOFLUX isoprene flux measurement and OMI HCHO were separately used to derive a drought stress factor γ_d which replaces γ_{SM} in Equation (1) to simulate the response of isoprene emissions to drought in MEGAN2.1 implementation of GEOS-Chem (hereafter referring to as GC/MEGAN2.1). The drought stress factor γ_d derived from the MOFLUX isoprene flux measurement is denoted as γ_{d_MOFLUX} and that from OMI HCHO as γ_{d_OMI}. Their corresponding simulations are referred to as MOFLUX_Stress_GC and OMI_Stress_GC, respectively. In either algorithm, the underlying assumption is that the GEOS-Chem model has no significant bias in predicting isoprene fluxes or HCHO columns due to factors other than isoprene emissions under drought conditions. The assumption is reasonable because the GEOS-Chem model uses

reanalysis meteorology, state-of-the-science isoprene oxidation schemes, time-specific anthropogenic emissions and fire emissions, and natural emissions calculated online using model meteorology as described in Section 2.3. The discussion in Section 3.1 validated some aspects of the assumption such as NOx emissions, wildfire emissions, and PBL.

4.1 MOFLUX-based Drought Stress Algorithm

The γ_{d_MOFLUX} was derived following Jiang et al. (2018) by implementing photosynthesis and water stress parameters with a formula of:

$$\gamma_{d\_MOFLUX} = \gamma_0 \gamma_{d\_isoprene} \begin{cases} \gamma_{d\_isoprene} = 1 \, (\beta_t \geq 0.3) \\ \gamma_{d\_isoprene} = V_{cmax}/\alpha \, (\beta_t < 0.3, \alpha = 77) \end{cases} \tag{2}$$

where V_{cmax} is the maximum carboxylation rate by photosynthetic Rubisco enzyme and β_t represents the water stress ranging from zero (fully stressed) to one (no stress). This simplified method intends to use the decreased photosynthetic enzyme activity to physiologically represent the variation in isoprene emissions under drought stress via dividing V_{cmax} by an empirical parameter α when the water stress is below a threshold.

Since the default GEOS-Chem does not have these photosynthetic parameters, we adopted the ecophysiology module created by Lam et al. (2022) that is based on the photosynthesis calculation in the Joint UK Land Environmental Simulator (JULES; Best et al., 2011; Clark et al., 2011) as an online component in GEOS-Chem so that it simulates photosynthesis rate and bulk stomatal conductance dynamically and consistently with the underlying meteorology that drives GEOS-Chem. The outputs of V_{cmax} and β_t from the ecophysiology module were passed to MEGAN2.1 in GEOS-Chem to parameterize the drought stress according to Equation 2. In addition to GEOS-Chem meteorology, the ecophysiology module uses soil parameters from the Hadley Centre Global Environment Model version 2 – Earth System Model (HadGEM2-ES). In general, the implementation of the ecophysiology module much improved the simulated stomatal conductance and dry deposition velocity relative to site observations on average for seasonal timescales, but the β_t computed has not been calibrated to intermittent drought conditions. Instead of adopting the values of V_{cmax} and β_t from Jiang et al. (2018) which were based on the Community Land Model, we need to determine the β_t threshold and the α value specific to GEOS-Chem with the ecophysiology module of Lam et al. (2022). To calibrate β_t, we first examined the statistical distribution of β_t at the MOFLUX grid (**Figure S2**) during May-September 2011 and 2012 when multiple USDM drought categories occurred. Then we decided on a value of 0.3 as the threshold β_t below which the drought stress will be triggered in the model because this value is greater than 75% quantile of all the β_t values from D0 to D3, thus capturing most of the drought conditions.

We note the observed isoprene flux at MOFLUX is consistently higher than predicted values during the non-drought period (e.g., N0 in Figure 5a). This systematic bias is expected because we compare the single-point observations with grid-mean isoprene emission fluxes. To correct the systemic bias, we scaled down the model isoprene emissions at the MOFLUX grid by a factor of 1.42, which is the ratio of the average hourly isoprene fluxes between observations and simulations at the MOFLUX grid during non-drought conditions ($\beta_t > 0.3$). The factor of 1.42 was applied to

345   downscale modeled isoprene fluxes at the MOFLUX grid during the entire time series, including drought conditions.

346   The resulted time series are shown in **Figure 6a**. Based on the downscaled model prediction, we derived that α=77

347   under drought conditions ($\beta_t < 0.3$), which minimized the mean bias under drought conditions between the modeled

348   and observed isoprene fluxes at the MOFLUX grid.

349   **Figure 6b** shows the comparison of the hourly NoStress_GC and MOFLUX_Stress_GC isoprene emissions with

350   observations in May-September 2012. The overall mean bias is reduced from 2.05 mg/m^2/hr to 0.01 mg/m^2/hr despite

351   the fact that the stress factor is only applied to drought conditions. The correlation coefficient (R) and index of

352   agreement (IOA) also increase from 0.77 to 0.85 and from 0.80 to 0.93, respectively. All the changes in the comparison

353   metrics indicate the model simulations are improved considerably based on the single-point measurement.

354
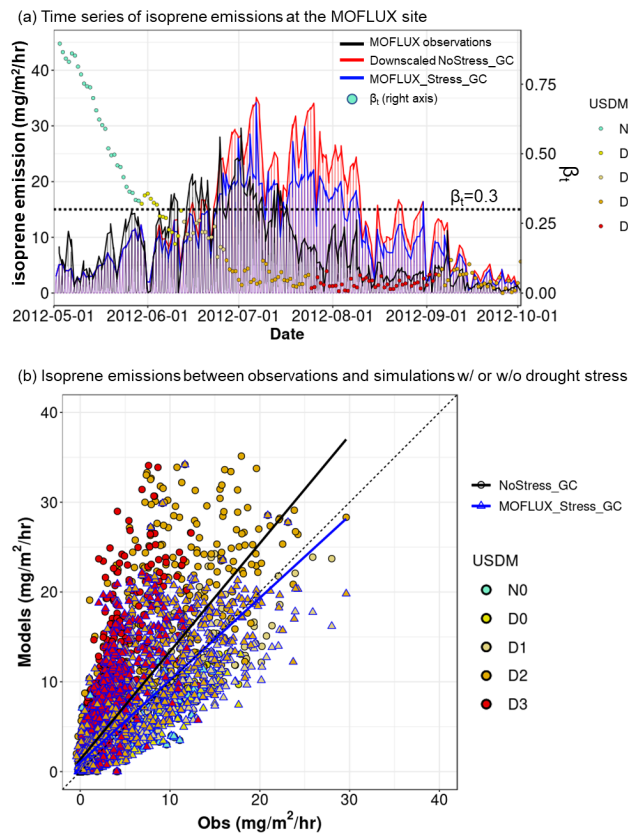
355   **Figure 6. (a) Hourly time series of isoprene emissions at the MOFLUX site from observations (black line) and simulations**
356   **with (MOFLUX_Stress_GC; blue line) and without drought stress (NoStress_GC; red line; after downscaling). The dots**
357   **color-coded by USDM levels represent the daily values of β_t (right axis). The dashed line indicates the threshold of 0.3. (b)**
358   **Comparison of isoprene emissions between observations (Obs) and simulations with (MOFLUX_Stress_GC; blue-bordered**
359   **triangle) and without (NoStress_GC; black-bordered circle) drought stress. Data are color-coded by USDM levels.**

 4.2 OMI-based Drought Stress Algorithm

361
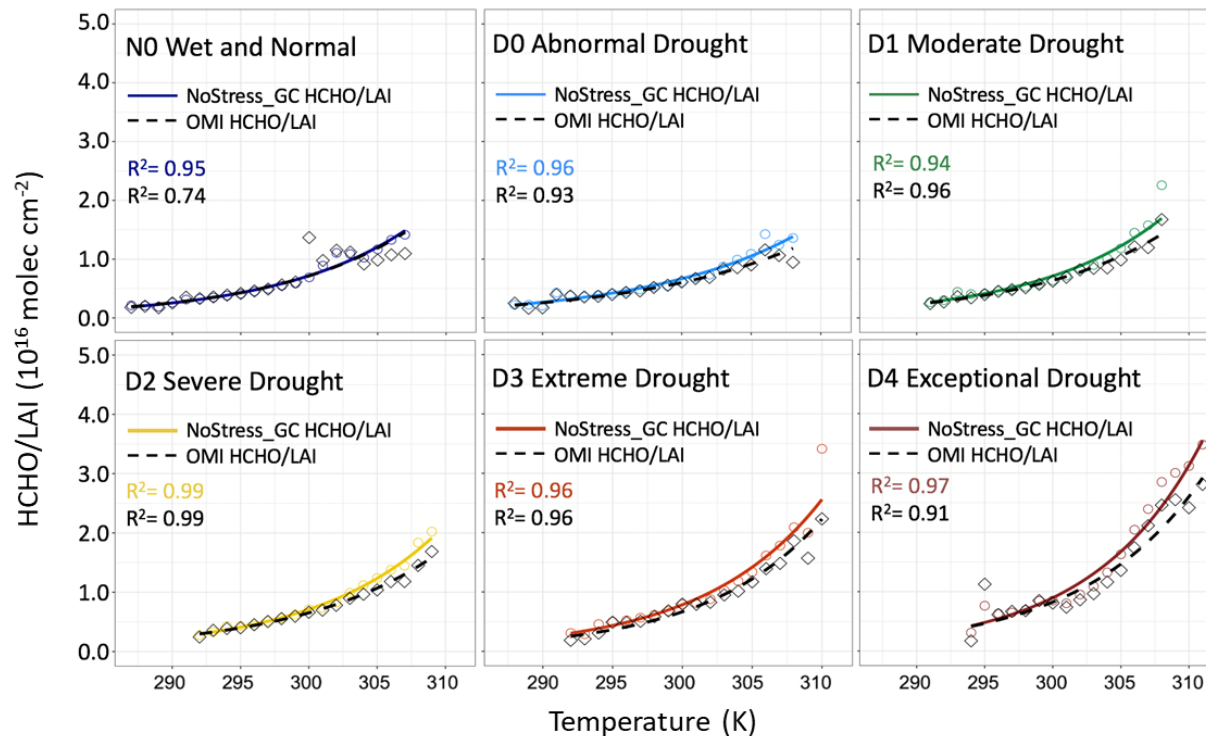
Figure 7. Response of HCHO/LAI ratio (10^{16} molec cm^{-2}) to temperature (K) in different drought levels averaged over JJA 2005-2017. The colored solid line is the modelled NoStress_GC HCHO/LAI ratio, and the black dashed line is the observed HCHO/LAI ratio from OMI. The exponentially fitted formulas and the resulted coefficient of determination (R^2) are labelled in each subplot.

Isoprene emission increases exponentially with temperatures below ~310 K (Guenther et al., 2006) in the absence of other stress factors such as drought. Indeed, an exponential relationship between biogenic isoprene emission per unit LAI and temperature is predicted by MEGAN2.1 at all USDM levels (**Figure S3**). However, the predicted temperature sensitivity is found to increase substantially with drought severity with no sign of plateauing or slow-down even under the most severe drought conditions when MOFLUX measurements measured a decrease in isoprene emissions (c.f. Figure 5). Similarly, we found NoStress_GC overestimates HCHO sensitivities to high temperatures (> 300 K) under drought conditions (D0-D4) (**Figure 7**), but no such overestimation is seen under non-drought (N0) or low temperature conditions during drought (< 300 K). This indicates the role of drought stress on isoprene emissions is likely through suppressing the dependence of emissions on temperatures during drought. Leaf level measurements conducted during the 2012 drought at the MOFLUX site provide independent evidence of drought suppression of the isoprene response to increasing temperature for less drought-resilient tree species (Geron et al., 2016). Taking advantage of these empirical observations, we derived the OMI-based drought stress algorithm by minimizing the differences in HCHO column sensitivities to temperatures between OMI and GEOS-Chem under drought conditions as shown in **Figure 7**. When calculating the relationships between HCHO column densities and temperatures, we first scaled HCHO column by LAI on a grid-by-grid basis to account for the regional differences in isoprene emissions due to different vegetation coverage as well as the effect of LAI changes with drought (c.f. **Figure 4**). Each point in **Figure 7** represents the mean

382 HCHO/LAI ratio, denoted as Ω, within each 1K temperature interval. We used exponential functions ($ln\Omega = kT + b$) to

383 separately fit the temperature (T) dependence of HCHO/LAI ratio (Ω) under different drought levels (**Figure 7**) for

384 both the model and OMI. The resulting formulas were listed in **Table 1** and the R^2 of most fitting lines is greater than

385 0.9.

386 **Table 1. Fitted exponential formulas of NoStress_GC and OMI HCHO/LAI ratio (Ω, 10^{16} molec cm^{-2}) to surface air**
387 **temperature (T, K), and fitted value of HCHO/LAI ratio at 290K, 300K, and 310K.**

USDM	NoStress_GC HCHO/LAI (Ω, 10^{16} molec cm^{-2})				OMI HCHO/LAI (Ω, 10^{16} molec cm^{-2})			
	Fitting Formula	290K	300K	310K	Fitting Formula	290K	300K	310K
N0	$ln\Omega = 0.104T - 31.42$	0.25	0.72	2.03*	$ln\Omega = 0.101T - 30.78$	0.26	0.72	1.97*
D0	$ln\Omega = 0.091T - 27.83$	0.27	0.67	1.66	$ln\Omega = 0.085T - 25.92$	0.26	0.60	1.40
D1	$ln\Omega = 0.108T - 32.83$	0.24	0.71	2.10	$ln\Omega = 0.100T - 30.56$	0.23	0.64	1.74
D2	$ln\Omega = 0.110T - 33.33$	0.24	0.71	2.14	$ln\Omega = 0.098T - 29.97$	0.24	0.65	1.75
D3	$ln\Omega = 0.118T - 35.72$	0.24	0.78	2.56	$ln\Omega = 0.121T - 36.62$	0.20	0.67	2.23
D4	$ln\Omega = 0.125T - 37.59$	0.26	0.90	3.13	$ln\Omega = 0.115T - 34.62$	0.26	0.83	2.60

388 * Asterisk indicates that the temperature does not reach this value in actual data and is an extrapolated value.

389 As the fitting equations suggest, both NoStress_GC and OMI HCHO/LAI ratios increase with temperature under all

390 conditions, but the former shows a higher sensitivity to temperature under drought conditions. This can be clearly seen

391 from the higher HCHO/LAI ratios of NoStress_GC (Ω_{GC}; solid lines) than those of OMI (Ω_{OMI}; dashed lines)

392 especially when the temperature is greater than 300 K under D0-D4. To better explain this, we also calculated the

393 fitted value of HCHO/LAI at three temperatures of 290K, 300K, and 310K in **Table 1**. Since it is difficult for the N0

394 condition to reach a temperature of 310K, the values were extrapolated and marked with an asterisk in the table. The

395 results show that the model overestimates the temperature dependence at all drought levels. At 290K, all biases

396 between Ω_{OMI} and Ω_{GC} are less than 0.05×10^{16} molec cm^{-2}. At 310K, the bias between the two is 0.06×10^{16} molec

397 cm^{-2} (3.0%) at N0 but increases by more than a factor of 4 to 0.26×10^{16} molec cm^{-2} (18.6%), 0.36×10^{16} molec cm^{-2}

398 (20.7%), 0.39×10^{16} molec cm^{-2} (22.3%), 0.33×10^{16} molec cm^{-2} (14.8%), and 0.53×10^{16} molec cm^{-2} (20.4%) at D0-

399 D4 drought, respectively. As isoprene emission is a fixed function of temperature in MEGAN2.1, the overdependence

400 of HCHO column on temperature is caused by the previous two weeks' temperatures being higher under drought,

401 which leads to a higher value of γ_T reflecting the temperature "memory" effects on isoprene emissions (**Figure S4**).

402 Based on the fitted formulas in **Table 1**, the ratio between $\frac{\Omega_{OMI}}{\Omega_{GC}}$ under each level from D0 to D4 can be derived by:

403 $$\frac{\Omega_{OMI}}{\Omega_{GC}} = \frac{e^{k_{OMI}T + b_{OMI}}}{e^{k_{GC}T + b_{GC}}} = e^{(k_{OMI} - k_{GC})T} e^{(b_{OMI} - b_{GC})}$$ (3)

404 where k_{OMI} (k_{GC}) and b_{OMI} (b_{GC}) represent the slopes and interpolations of the formulas in **Table 1** for OMI (GC)

405 HCHO column; T is surface temperature, and e is the exponential constant. By averaging the values of k_{OMI}-k_{GC} and

406 b_{OMI}-b_{GC} from D0 to D4, we can obtain:

407 $$\frac{\Omega_{OMI}}{\Omega_{GC}} = 380.10e^{-0.02T} \ (\beta_t < 0.6, T > 300\ K)$$ (4)

408 where $\beta_t < 0.6$ represents the 75% quantile of the β_t values from D0 to D4 for the whole SE US study region in JJA

409 2005-2017 (**Figure S2**).

410 The formula of γ_{d_OMI} is thus:

411 $$\gamma_{d\_OMI} = \gamma_0\gamma_{d\_isoprene} \begin{cases} \gamma_{d\_isoprene} = 1 \ (\beta_t \geq 0.6 \ or \ T \leq 300K) \\ \gamma_{d\_isoprene} = \frac{\Omega_{OMI}}{\Omega_{GC}} = 380.10e^{-0.02T} \ (\beta_t < 0.6, T > 300K) \end{cases}$$ (5)

412 Note the threshold of β_t in equation 5 is different from the value used by γ_{d_MOFLUX} because all the SE US grids were

413 considered in deriving β_t for γ_{d_OMI}. Another difference is that the factor is activated only if the temperature is higher

414 than 300K when significant biases between Ω_{OMI} and Ω_{GC} are found (**Figure 7**).

415
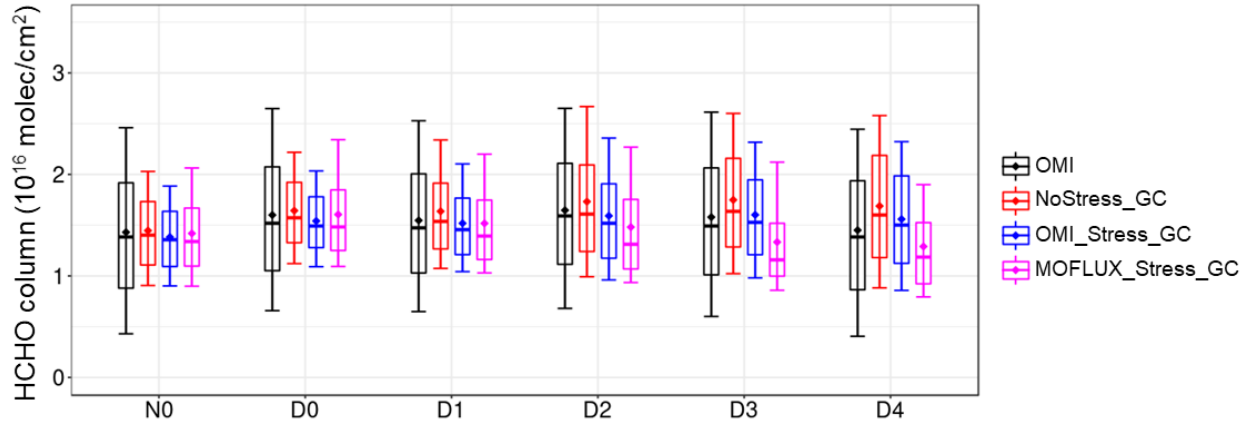
416 **Figure 8. Boxplot of HCHO column statistical distributions for OMI observations (black) and different GEOS-Chem**
417 **simulations: without drought stress (NoStress_GC; red) and with drought stress factors derived from MOFLUX**
418 **observations (MOFLUX_Stress_GC; blue) and from OMI HCHO constraints (OMI_Stress_GC; pink).**

419 **Figure 8** compares the statistical distributions of HCHO column densities from OMI, NoStress_GC,

420 MOFLUX_Stress_GC, and OMI_Stress_GC during May-September 2012 over the SE US. Compared to OMI,

421 NoStress_GC simulation has a mean high bias of 0.02×10^{16} molec cm^{-2} - 0.24×10^{16} molec cm^{-2} during D0-D4. The

422 γ_{d_OMI} algorithm reduces the high bias to -0.05×10^{16} molec cm^{-2} - 0.11×10^{16} molec cm^{-2}. By contrast, the γ_{d_MOFLUX}

423 algorithm reduces the HCHO simulations too much over the SE US and causes an overall underestimation of 0.02×10^{16}

424   molec cm^{-2} - 0.25×10^{16} molec cm^{-2}. The γ_{d_MOFLUX} algorithm also narrows the statistical distribution of HCHO as

425   indicated by the smaller boxes and shorter whiskers compared to OMI. This suggests that the γ_{d_MOFLUX} algorithm

426   based on the single-site observations is incapable of representing the drought stress over the SE US, possibly because

427   the MOFLUX site has thin soil layers and thus is vulnerable to water stress (Opacka et al., 2022). Isoprene emissions

428   measured here are therefore more sensitive to droughts and the same extent of drought stress is likely too strong to be

429   applied to other regions in the SE US. As a result, the γ_{d_OMI} algorithm is used in the next section to further evaluate

430   how this algorithm would change the responses of atmospheric compositions to droughts.

431   **5. Changes in Simulated Biogenic Isoprene Emissions, HCHO, O$_3$, and OA**

432   In this section, we evaluated the changes in biogenic isoprene emissions and HCHO column densities by running a

433   long-term (2005-2017, JJA) simulation, after adding the OMI-based drought stress factor for isoprene emissions γ_{d_OMI}

434   in GEOS-Chem. Since isoprene is an important precursor for the formation of tropospheric O$_3$ and OA, maximum

435   daily 8-hour average (MDA8) O$_3$, and OA changes were also examined. We used the ComplexSOA mechanism in

436   GEOS-Chem (Pye et al., 2010; Marais et al., 2016) which includes more detailed pathways of isoprene to secondary

437   organic aerosols such as aqueous-phase reactive uptake and the formation of organo-nitrates.

438   **Figure 9** shows the changes in biogenic isoprene emissions resulting from adding γ_{d_OMI} drought stress in GEOS-

439   Chem. Here we expanded the maps to the entire contiguous US to examine whether the drought stress algorithm can

440   impose large changes on other US regions although such changes need to be interpreted with caution. The numbers at

441   each panel indicate the means of isoprene emissions of NoStress_GC and the mean differences (MD) relative to the

442   OMI_Stress_GC over the SE US. As expected, the biggest decrease in isoprene emissions is found in the SE US with

443   the regional-mean emissions reduced by 0.17×10^{-10} kg m^{-2} s^{-1} (8.60%), 0.35×10^{-10} kg m^{-2} s^{-1} (14.24%), 0.43×10^{-10} kg

444   m^{-2} s^{-1} (16.57%), 0.49×10^{-10} kg m^{-2} s^{-1} (17.49%), 0.58×10^{-10} kg m^{-2} s^{-1} (18.66%), and 0.65×10^{-10} kg m^{-2} s^{-1} (20.74%)

445   from N0 to D4, respectively (**Figure 9c**). Despite lowering emissions relative to NoStress_GC, OMI_Stress_GC

446   simulates an increase of isoprene emissions under drought conditions compared to non-drought in the SE US; the

447   respective increases are 0.28×10^{-10} kg m^{-2} s^{-1} (15.20%), 0.34×10^{-10} kg m^{-2} s^{-1} (18.40%), 0.49×10^{-10} kg m^{-2} s^{-1} (26.47%),

448   0.69×10^{-10} kg m^{-2} s^{-1} (37.46%), and 0.65×10^{-10} kg m^{-2} s^{-1} (35.23%) from D0 to D4 relative to N0 (**Figure 9c**). This

449   increase results from the top-down constraints by the corresponding changes in OMI HCHO column densities with

450   USDM and consequently exhibits the behavior of non-uniform increases with drought severity (e.g., peak increase of

451   37.5% at D3, followed by a ~2% reduction at D4), which is consistent with the MOFLUX flux measurements.

452   For other regions, such as California and Minnesota, biogenic isoprene emissions decreased slightly by less than

453   0.5×10^{10} kg m^{-2} s^{-1}. The smaller effect of the drought stress factor imposed on regions other than the SE US is

454   understandable because of the lower isoprene emissions.
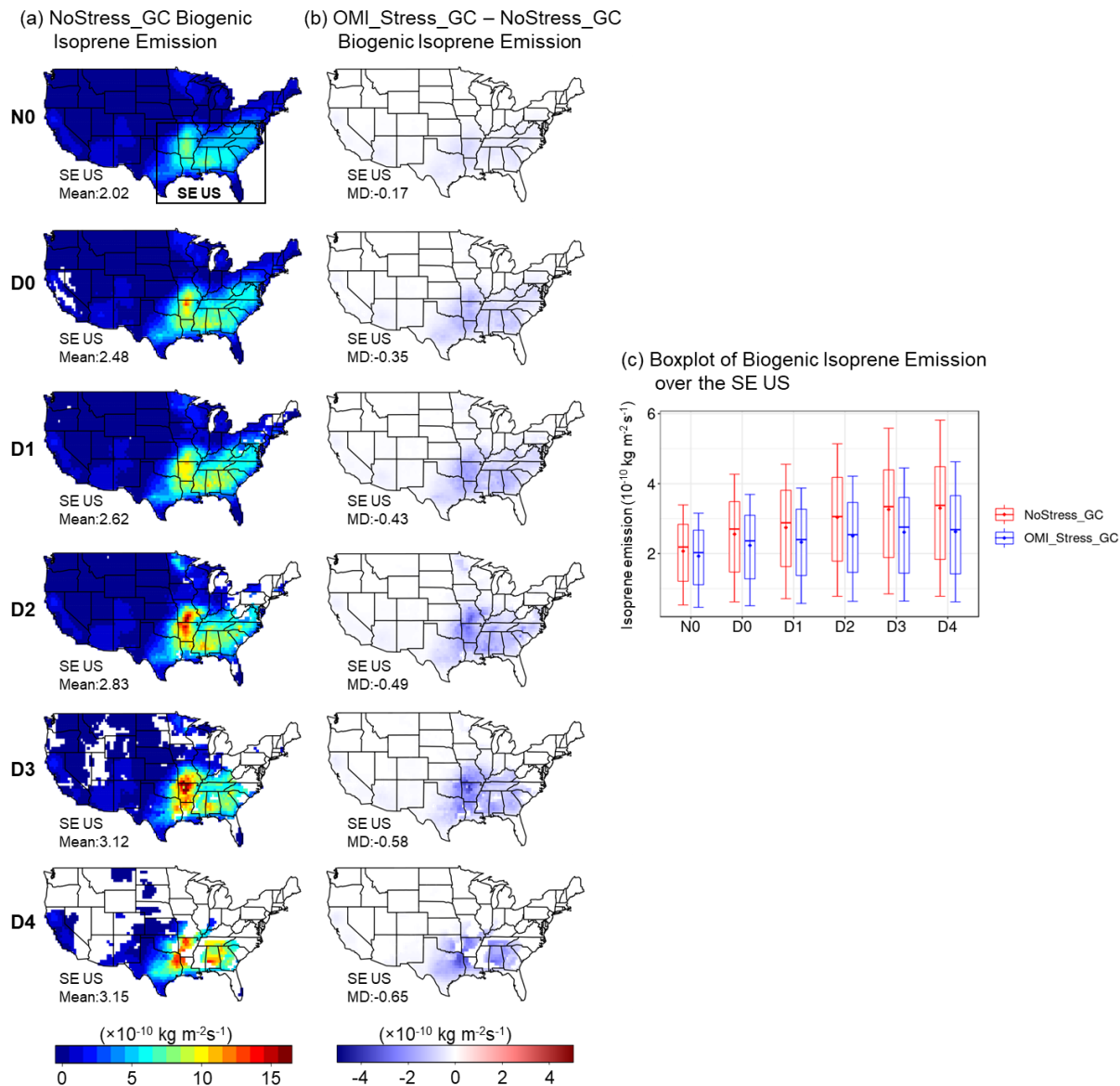
Figure 9. Simulated biogenic isoprene emissions during JJA 2005-2017 by USDM dryness category by NoStress_GC (a), OMI_Stress_GC minus NoStress_GC (b), and statistical distributions of SE US isoprene emissions between the two simulations (c). Numbers at the bottom-left corner of each panel indicate the SE US (black box) regional mean of biogenic isoprene emissions for NoStress_GC (left column), and mean differences (MD) between OMI_Stress_GC and NoStress_GC (middle column).

455

456
457
458
459
460
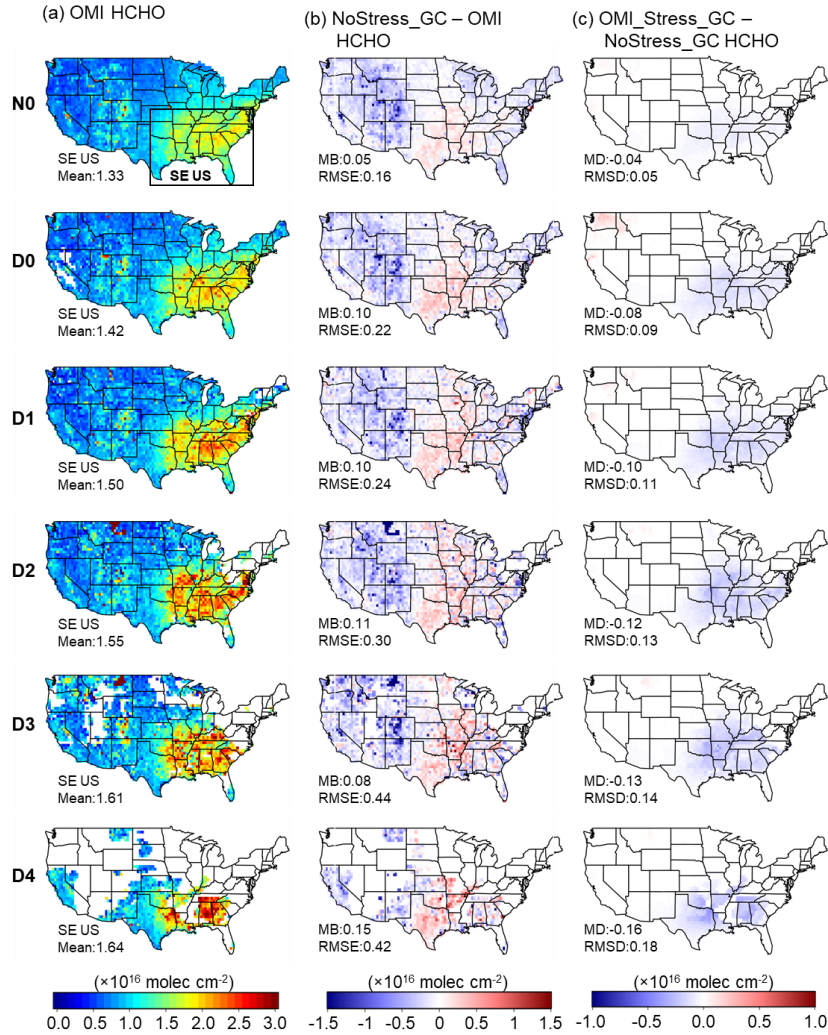
Figure 10. Mean HCHO column densities during JJA 2005-2017 by USDM dryness category for OMI (a), NoStress_GC minus OMI (b), and OMI_Stress_GC minus NoStress_GC (c). Numbers at the bottom-left corner of each panel indicate the SE US (black box) regional mean of OMI HCHO column (left column), mean bias (MB), and root mean square error (RMSE) in HCHO column densities between NoStress_GC and OMI (middle column), and mean differences (MD) and root mean square deviation (RMSD) between OMI_Stress_GC and NoStress_GC (right column). MD and RMSD are calculated in the same way as MB and RMSE; the different names are used to distinguish between model-to-model comparison and model-to-observation comparison, respectively.

The changes in the HCHO column are shown in **Figure 10**. Different from the overestimation in the SE US, NoStress_GC underestimates HCHO column densities in the western US compared to OMI (**Figure 10b**). This negative bias should be interpreted with care because the scaling factor of 1.5 (c.f. section 2.2) is derived over the SE US and may not hold in other regions. For the SE US overall, the drought stress factor reduces modeled HCHO columns by 0.08×10^{16} molec cm^{-2} (5.43%), 0.10×10^{16} molec cm^{-2} (6.46%), 0.12×10^{16} molec cm^{-2} (7.22%) and 0.13×10^{16} molec cm^{-2} (7.62%), 0.16×10^{16} molec cm^{-2} (8.91%) under D0-D4, respectively, relative to NoStress_GC (**Figure 10c**). This leads to a better agreement with OMI as OMI_Stress_GC has nearly zero MB under D0-D4 (**Figure S5**; MB = -0.05×10^{16} molec cm^{-2} $\sim0.02\times10^{16}$ molec cm^{-2}). The RMSE is also reduced by 3%-13% relative to the NoStress_GC simulation compared to observations. The changes in both metrics indicate that the drought algorithm

478 considerably improves the model performance in capturing the biogenic isoprene response to drought as evidenced by

479 HCHO column. Similar to the changes in biogenic isoprene emissions, the OMI_Stress_GC only slightly decreases

480 HCHO column densities (<5%) compared to the NoStress_GC simulation in other US regions.

481
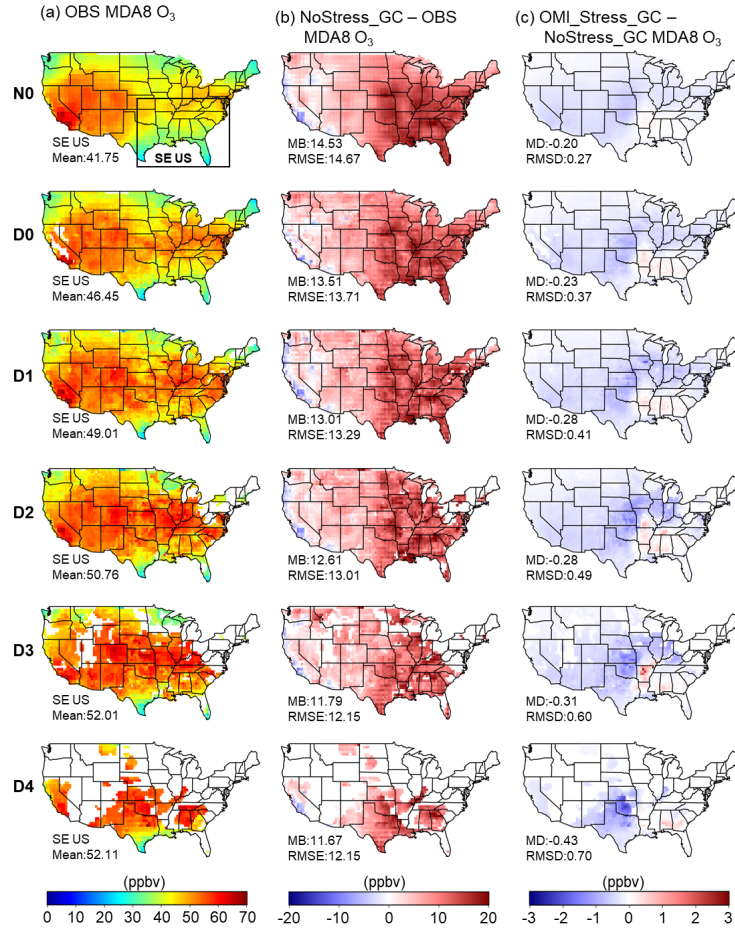
Figure 11. Same as Figure 10 but for surface maximum daily 8-hour average (MDA8) O$_3$.

483 **Figure 11a** displays the observed MDA8 O$_3$ changes with USDM. Similar to the changes of the HCHO column with

484 USDM levels, O$_3$ in the SE US exhibits a gradual increase, relative to the mean of 41.74 ppbv at N0, of 4.70 ppbv,

485 7.26 ppbv, 9.01 ppbv, 10.26 ppb, and 10.36 ppbv under D0-D4, respectively. This is consistent with our previous

486 study (Li et al., 2022; Lei et al., 2022) which investigated O$_3$ changes with drought severity in more detail. The

487 NoStress_GC simulation has a high bias in MDA8 O$_3$ across all USDM categories (**Figure 11b**). High positive bias

488 is a common issue of surface O$_3$ simulations in chemical transport models, which is a research question and can be

489 attributed to the uncertainties in various processes, such as NO$_x$ emissions, isoprene oxidation pathways, O$_3$ dry

490 deposition velocity, boundary layer dynamics (Fiore et al., 2005; Lin et al., 2008; Squire et al., 2015; Travis et al.,

491 2016; Travis and Jacob, 2019). Despite the systematic high bias, NoStress_GC captures the increasing trend of MDA8

492 O$_3$ with increasing dryness but with a respectively smaller increment (relative to N0) of 3.62 ppbv, 5.67 ppbv, 7.01

493 ppbv, 7.41 ppbv, and 7.41 ppbv under D0 to D4. This discrepancy between NoStress_GC and observations can also

494   be inferred from the fact that the MB between model and observations decreases from 14.53 ppbv at N0 to 11.67 ppbv

495   at D4 (**Figure 11b**). **Figure 11c** shows the difference in MDA8 O_3 between OMI_Stress_GC and NoStress_GC. In

496   the SE US where isoprene emissions are the highest and reduced the most by the drought stress algorithm,

497   OMI_Stress_GC shows a small increase in MDA8 O_3 of less than 1 ppbv. This increase in O_3 can be explained by an

498   increase of OH resulting from reducing isoprene emissions under low-NO_x conditions in the SE US (Wells et al.,

499   2020). For the SE US study domain as a whole, the change in MDA8 ozone was negligible but negative (regional

500   mean of -0.5 ppbv). Although the drought factor does not reduce the overall high bias, it makes the model more

501   consistent with the observed increment in MDA8 O_3 for the subregion with increased O_3 (e.g., 90–94°W, 32–35°N) as

502   drought severity increases. Since NO_x has a high positive bias from the NEI2011 inventory (**Figure 4**), the

503   improvement of MDA8 in these regions is likely to be underestimated. Over northeastern Texas, Oklahoma, and

504   Kansas where isoprene emission is also reduced by the drought algorithm yet from a much lower emission base

505   compared to other SE US areas, OMI_Stress_GC simulates 1-3 ppbv lower MDA8 O_3 under drought conditions (D0-

506   D4), leading to a better agreement with observations. For regions with lower isoprene and higher NO_x concentrations,

507   O_3 formation is more sensitive to the changes in isoprene, which explains the reduction in MDA8 O_3 caused by the

508   drought stress factor.

509
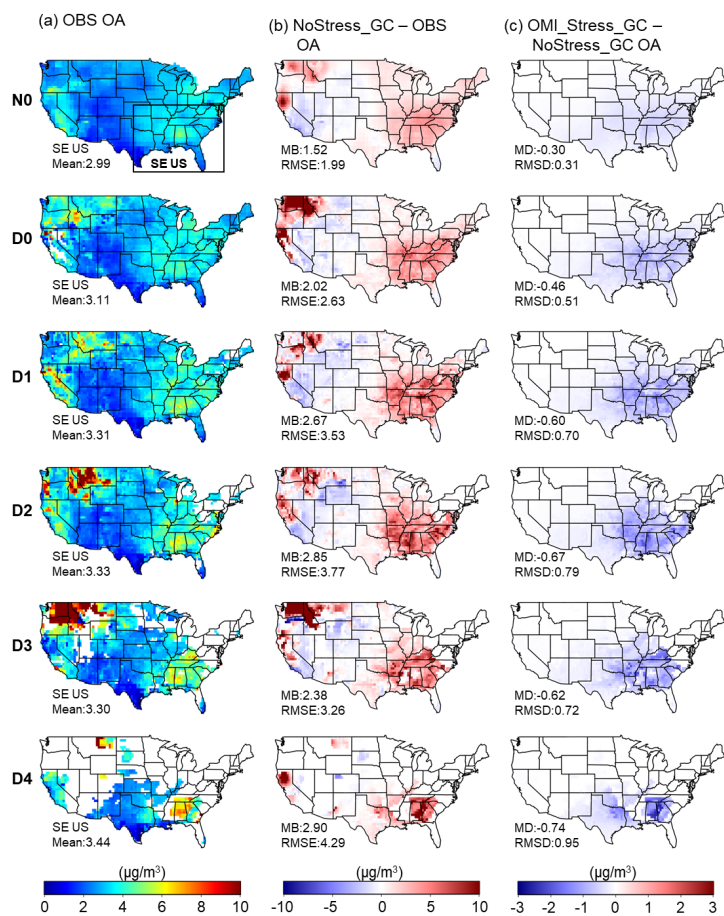
510   **Figure 12. Same as Figure 10 but for organic aerosol (OA).**

511   The changes in OA with USDM are shown in **Figure 12.** Observed OA in the SE US shows an average increase

512   (relative to N0) of 0.12 μg/m³, 0.32 μg/m³, 0.34 μg/m³, 0.31 μg/m³, and 0.45 μg/m³ under D0 to D4, respectively. The

513   extremely high values over the northwest states (e.g., Washington and Montana) are likely associated with higher

514   wildfire emissions under droughts (Wang et al., 2017). The NoStress_GC simulation considerably overestimates OA

515   in the SE US with an MB of 1.52 μg/m³ (50.83%) at N0 and the overestimation becomes even higher to 2.02-2.90

516   μg/m³ (64.95%-85.58%) at D0-D4 (**Figure 12b**), thus causing an overprediction of the drought-OA relationship.

517   Zheng et al (2020) reported a similar level of overestimation and attributed this to the overdependence of isoprene-

518   derived secondary organic aerosol (SOA) on sulfate. As isoprene is one of the dominant sources of OA in the SE US

519   (Xu et al., 2015; Budisulistiorini et al., 2016), our analysis suggests that the model overestimation of isoprene

520   emissions under drought conditions is another reason for this high OA bias in the SE US. Indeed, the drought stress

521   factor greatly improves the OA simulation by reducing the MB by 0.30 μg/m³ (6.60%), 0.46 μg/m³ (8.98%) 0.60

522   μg/m³ (10.07%), 0.67 μg/m³ (10.85%), 0.62 μg/m³ (10.88%), 0.74 μg/m³ (11.71%) under N0 to D4 over the SE US

523   relative to NoStress_GC, thus lowering the MB to be within 1.22-2.18 μg/m³ (40.82% - 65.52%; **Figure S5**) compared

524   with observations. We also examined the change of three major SOA components in **Figure S6**. Anthropogenic SOA

525   (ASOA) barely changes; isoprene SOA (ISOA) decreases the most as expected since the drought stress factor is

526   applied to isoprene emissions only. Interestingly, terpene SOA (TSOA) also shows a slight decrease, suggesting

527   positive feedback between ISOA and TSOA.

528   In summary, the OMI-based drought stress factor shows good performance in correcting the overestimation of

529   biogenic isoprene in default GEOS-Chem simulations under drought conditions. The drought stress factor was

530   constrained by the observed exponential fitting between the HCHO to LAI ratio and temperature, not by observed

531   HCHO columns directly. It nearly eliminates the high HCHO bias compared with OMI observations in the SE US

532   under drought conditions, which consequently improves the simulation of OA. MDA8 O_3 slightly increases in the

533   areas with high isoprene emissions, leading to no improvement in model bias but a better agreement with the observed

534   O_3 increment with drought severity. Places with lower isoprene emissions show an MDA8 O_3 reduction of 1-3 ppbv,

535   indicating the region-specific O_3 responses to the changes of isoprene due to the nonlinearity of O_3 chemistry.

536   **6. Conclusions**

537   Using long-term (JJA 2005-2017) weekly USDM drought index and OMI HCHO column data over the SE US, we

538   revealed a step-increase pattern of HCHO by 6.7%, 12.6%, 16.5%, 21.2%, and 23.2% from D0 to D4 relative to non-

539   drought conditions (N0), respectively, which indicates the increasingly higher isoprene emissions with drought on a

540   regional scale although the rate of increase decreases under severe droughts. Compared with OMI observations, the

541   GEOS-Chem simulated HCHO column density exhibits a similar pattern, but the changes are 1.1-1.5 times higher

542   with a respective increase of 9.90%, 15.1%, 19.5%, 21.8%, and 29.1% from D0 to D4. Since there are no big changes

543   in anthropogenic VOCs under droughts, biogenic isoprene emissions are the key drivers for the increase of HCHO,

544   and a drought stress factor is missing in the MEGAN2.1 biogenic inventory in the default GEOS-Chem simulations

545   causing the overestimation of the HCHO changes in response to droughts.

546 The MOFLUX site provides the only long-term ground-based isoprene flux observations covering multiple drought

547 severities. We developed a drought stress algorithm based on the MOFLUX site following Jiang et al. (2018), and the

548 algorithm improves the HCHO simulation at the MOFLUX grid while underestimating HCHO after all the SE US

549 grids are included. By comparison, the OMI-based drought stress algorithm derived from the different HCHO-

550 temperature sensitivities between OMI and GEOS-Chem can reflect better spatial coverage and nearly removes the

551 positive bias between OMI and the default simulations seen from a test simulation in May-September 2012 over the

552 SE US.

553 The long-term simulation with the OMI-based drought stress factor can significantly reduce the biogenic isoprene

554 emissions by 0.35×10^{-10} kg m^{-2} s^{-1} (14.24%), 0.43×10^{-10} kg m^{-2} s^{-1} (16.57%), 0.49×10^{-10} kg m^{-2} s^{-1} (17.49%), 0.58×10^{-10}

555 ^{10} kg m^{-2} s^{-1} (18.66%) and 0.65×10^{-10} kg m^{-2} s^{-1} (20.74%) from D0 to D4, respectively, which consequently leads to a

556 better agreement between OMI and simulated HCHO column. Despite lowering emissions relative to the no-stress

557 simulation, OMI_Stress_GC simulates a non-uniform trend of increasing isoprene emissions with drought severity

558 that is consistent with OMI HCHO and MOFLUX. Relative to N0, the simulated increase in isoprene emissions is 15-

559 18% under D0-D1, increasing to 26% at D2 and peaking at 37% at D3, followed by a slight decrease to 35% at D4.

560 The observed MDA8 O_3 and OA over the SE US show a similar increase pattern with HCHO. The OMI-based drought

561 stress algorithm also helps reduce the mean bias of OA by 0.30 μg/m^3 (6.60%), 0.46 μg/m^3 (8.98%) 0.60 μg/m^3

562 (10.07%), 0.67 μg/m^3 (10.85%), 0.62 μg/m^3 (10.88%), 0.74 μg/m^3 (11.71%) from N0 to D4 over the SE US compared

563 with the high positive bias of more than 2.02 μg/m^3 (50.83%) without the drought stress. By contrast, the MDA8 O_3

564 response to the reduced biogenic isoprene caused by the drought stress factor presents a spatial disparity due to the

565 nonlinear O_3 chemistry. Places with high isoprene emissions show an increase of MDA8 O_3 by less than 1 ppbv, which

566 slightly improves the simulated drought-O_3 relationship. For the regions with low isoprene emissions in the SE US,

567 the drought stress factor reduces MDA8 O_3 by 1-3 ppbv.

568 This study reveals an increasingly higher level of biogenic isoprene under drought conditions over the regions with

569 high vegetation coverage. As drought is predicted to become more frequent in a warming climate (Cook et al., 2018),

570 it is essential to update current biogenic emission inventories by adding a drought stress factor and to improve the

571 constraints of isoprene chemistry in the climate chemistry models in order to have a better projection of air quality in

572 the future. We demonstrate the feasibility of applying satellite data to the development of drought stress algorithms

573 when ground-based measurements are limited. Our attempt here is a top-down approach and used temperature as the

574 only parameter to adjust isoprene emissions under drought conditions. The water stress threshold in our algorithm is

575 used only as a triggering parameter; that is, it is used to determine whether a grid is in drought or not and thus can be

576 replaced with other drought-identifying approaches. One issue with our approach is the type of temperature data to be

577 used in the algorithm. Ideally, it should be leaf temperature because this is what regulates stomata at the process level.

578 However, leaf temperature is not readily available from meteorological fields that drive CTMs. MEGAN uses 2 m air

579 temperature to parameterize isoprene emissions, and thus our algorithm uses the same temperature. More biogenic

580 emission flux observations covering different vegetation types and drought severities will be helpful to better depict

581 the relationships between biogenic VOCs and drought stress.

582 **Acknowledgment**

583 This work was supported by NASA Atmospheric Composition Modeling and Analysis Program (80NSSC19K0986).

584 The development of the ecophysiology module in GEOS-Chem has also been supported by the General Research Fund

585 (14306220) granted by the Hong Kong Research Grants Council. The authors thank NASA Langley Research Center

586 for the OMI HCHO column data and the National Drought Mitigation Center for making and providing the USDM

587 maps. Roger Seco was supported by grants RYC2020-029216-I and CEX2018-000794-S funded by

588 MCIN/AEI/10.13039/501100011033 and by the European Social Fund "ESF Investing in your future".

589 **Data Availability**

590 GEOS-Chem model is publicly available at http://www.geos-chem.org. LAI is obtained from

591 http://geoschemdata.wustl.edu/ExtData/HEMCO/Yuan_XLAI/v2021-06/. O_3 and organic carbon observational data

592 can be downloaded via https://aqs.epa.gov/aqsweb/documents/data_mart_welcome.html. Observational isoprene

593 measurements at MOFLUX are from Potosnak et al. 2014 and Seco et al. 2015 and are available upon request from

594 co-author Alex Guenther. Satellite ΩHCHO is available publicly at

595 https://cmr.earthdata.nasa.gov/search/concepts/C1626121562-GES_DISC.html.

596 **Competing interests**

597 The authors declare that they have no conflict of interest.

598 **Author contributions**

599 YW conceived the research idea. NL and WL conducted the model simulation and data analysis. JCYL and APKT

600 created the ecophysiology module. AG, MJP and RS provided the field observations. All authors contributed to the

601 interpretation of the results and the preparation of the manuscript

602 **References**

603 Abbot, D. S., Palmer, P. I., Martin, R. V., Chance, K. V., Jacob, D. J., and Guenther, A.: Seasonal and interannual
604 variability of North American isoprene emissions as determined by formaldehyde column measurements from
605 space, Geophys. Res. Lett., 30, https://doi.org/10.1029/2003GL017336, 2003.

606 Alvarado, L. M. A., Richter, A., Vrekoussis, M., Hilboll, A., Kalisz Hedegaard, A. B., Schneising, O., and Burrows,
607 J. P.: Unexpected long-range transport of glyoxal and formaldehyde observed from the Copernicus Sentinel-5
608 Precursor satellite during the 2018 Canadian wildfires, Atmospheric Chem. Phys., 20, 2057–2072,
609 https://doi.org/10.5194/acp-20-2057-2020, 2020.

610   Atkinson, R.: Atmospheric chemistry of VOCs and NOx, Atmos. Environ., 34, 2063–2101,
611   https://doi.org/10.1016/S1352-2310(99)00460-4, 2000.

612   Best, M. J., Pryor, M., Clark, D. B., Rooney, G. G., Essery, R. L. H., Ménard, C. B., Edwards, J. M., Hendry, M. A.,
613   Porson, A., Gedney, N., Mercado, L. M., Sitch, S., Blyth, E., Boucher, O., Cox, P. M., Grimmond, C. S. B., and
614   Harding, R. J.: The Joint UK Land Environment Simulator (JULES), model description – Part 1: Energy and water
615   fluxes, Geosci. Model Dev., 4, 677–699, https://doi.org/10.5194/gmd-4-677-2011, 2011.

616   Budisulistiorini, S. H., Baumann, K., Edgerton, E. S., Bairai, S. T., Mueller, S., Shaw, S. L., Knipping, E. M., Gold,
617   A., and Surratt, J. D.: Seasonal characterization of submicron aerosol chemical composition and organic aerosol
618   sources in the southeastern United States: Atlanta, Georgia,and Look Rock, Tennessee, Atmospheric Chem. Phys.,
619   16, 5171–5189, https://doi.org/10.5194/acp-16-5171-2016, 2016.

620   Chance, K.: OMI/Aura Formaldehyde (HCHO) Total Column Daily L3 Weighted Mean Global 0.1 deg Lat/Lon
621   Grid V003, Goddard Earth Sci. Data Inf. Serv. Cent. GES DISC Greenbelt MD USA, 2019.

622   Chang, K.-Y., Xu, L., Starr, G., and Paw U, K. T.: A drought indicator reflecting ecosystem responses to water
623   availability: The Normalized Ecosystem Drought Index, Agric. For. Meteorol., 250–251, 102–117,
624   https://doi.org/10.1016/j.agrformet.2017.12.001, 2018.

625   Chen, L. G., Gottschalck, J., Hartman, A., Miskus, D., Tinker, R., and Artusa, A.: Flash Drought Characteristics
626   Based on U.S. Drought Monitor, Atmosphere, 10, 498, https://doi.org/10.3390/atmos10090498, 2019.

627   Claeys, M., Graham, B., Vas, G., Wang, W., Vermeylen, R., Pashynska, V., Cafmeyer, J., Guyon, P., Andreae, M.
628   O., Artaxo, P., and Maenhaut, W.: Formation of Secondary Organic Aerosols Through Photooxidation of Isoprene,
629   Science, 303, 1173–1176, https://doi.org/10.1126/science.1092805, 2004.

630   Clark, D. B., Mercado, L. M., Sitch, S., Jones, C. D., Gedney, N., Best, M. J., Pryor, M., Rooney, G. G., Essery, R.
631   L. H., Blyth, E., Boucher, O., Harding, R. J., Huntingford, C., and Cox, P. M.: The Joint UK Land Environment
632   Simulator (JULES), model description – Part 2: Carbon fluxes and vegetation dynamics, Geosci. Model Dev., 4,
633   701–722, https://doi.org/10.5194/gmd-4-701-2011, 2011.

634   Cook, B. I., Mankin, J. S., and Anchukaitis, K. J.: Climate Change and Drought: From Past to Future, Curr. Clim.
635   Change Rep., 4, 164–179, https://doi.org/10.1007/s40641-018-0093-2, 2018.

636   Ferracci, V., Bolas, C. G., Freshwater, R. A., Staniaszek, Z., King, T., Jaars, K., Otu-Larbi, F., Beale, J., Malhi, Y.,
637   Waine, T. W., Jones, R. L., Ashworth, K., and Harris, N. R. P.: Continuous Isoprene Measurements in a UK
638   Temperate Forest for a Whole Growing Season: Effects of Drought Stress During the 2018 Heatwave, Geophys.
639   Res. Lett., 47, e2020GL088885, https://doi.org/10.1029/2020GL088885, 2020.

640   Fiore, A. M., Horowitz, L. W., Purves, D. W., Levy II, H., Evans, M. J., Wang, Y., Li, Q., and Yantosca, R. M.:
641   Evaluating the contribution of changes in isoprene emissions to surface ozone trends over the eastern United States,
642   J. Geophys. Res. Atmospheres, 110, https://doi.org/10.1029/2004JD005485, 2005.

643   Geron, C., Daly, R., Harley, P., Rasmussen, R., Seco, R., Guenther, A., Karl, T., and Gu, L.: Large drought-induced
644   variations in oak leaf volatile organic compound emissions during PINOT NOIR 2012, Chemosphere, 146, 8–21,
645   https://doi.org/10.1016/j.chemosphere.2015.11.086, 2016.

646   Giglio, L., Randerson, J. T., and van der Werf, G. R.: Analysis of daily, monthly, and annual burned area using the
647   fourth-generation global fire emissions database (GFED4), J. Geophys. Res. Biogeosciences, 118, 317–328,
648   https://doi.org/10.1002/jgrg.20042, 2013.

649   Guenther, A., Karl, T., Harley, P., Wiedinmyer, C., Palmer, P. I., and Geron, C.: Estimates of global terrestrial
650   isoprene emissions using MEGAN (Model of Emissions of Gases and Aerosols from Nature), Atmospheric Chem.
651   Phys., 6, 3181–3210, https://doi.org/10.5194/acp-6-3181-2006, 2006.

Guenther, A. B., Zimmerman, P. R., Harley, P. C., Monson, R. K., and Fall, R.: Isoprene and monoterpene emission rate variability: Model evaluations and sensitivity analyses, J. Geophys. Res. Atmospheres, 98, 12609–12617, https://doi.org/10.1029/93JD00527, 1993.

Guenther, A. B., Jiang, X., Heald, C. L., Sakulyanontvittaya, T., Duhl, T., Emmons, L. K., and Wang, X.: The Model of Emissions of Gases and Aerosols from Nature version 2.1 (MEGAN2.1): an extended and updated framework for modeling biogenic emissions, Geosci. Model Dev., 5, 1471–1492, https://doi.org/10.5194/gmd-5-1471-2012, 2012.

Guenther, A. B., Shah, T., and Huang, L.: A next generation modeling system for estimating Texas biogenic VOC emissions [M], AQRP Proj., 16–011, 2017.

Guo, J., Zhang, J., Yang, K., Liao, H., Zhang, S., Huang, K., Lv, Y., Shao, J., Yu, T., Tong, B., Li, J., Su, T., Yim, S. H. L., Stoffelen, A., Zhai, P., and Xu, X.: Investigation of near-global daytime boundary layer height using high-resolution radiosondes: first results and comparison with ERA5, MERRA-2, JRA-55, and NCEP-2 reanalyses, Atmospheric Chem. Phys., 21, 17079–17097, https://doi.org/10.5194/acp-21-17079-2021, 2021.

Guttman, N. B.: Accepting the Standardized Precipitation Index: A Calculation Algorithm1, JAWRA J. Am. Water Resour. Assoc., 35, 311–322, https://doi.org/10.1111/j.1752-1688.1999.tb03592.x, 1999.

Hoerling, M., Eischeid, J., Kumar, A., Leung, R., Mariotti, A., Mo, K., Schubert, S., and Seager, R.: Causes and Predictability of the 2012 Great Plains Drought, Bull. Am. Meteorol. Soc., 95, 269–282, https://doi.org/10.1175/BAMS-D-13-00055.1, 2014.

Huang, J., Dool, H. M. van den, and Georgarakos, K. P.: Analysis of Model-Calculated Soil Moisture over the United States (1931–1993) and Applications to Long-Range Temperature Forecasts, J. Clim., 9, 1350–1362, https://doi.org/10.1175/1520-0442(1996)009<1350:AOMCSM>2.0.CO;2, 1996.

Huang, L., McGaughey, G., McDonald-Buller, E., Kimura, Y., and Allen, D. T.: Quantifying regional, seasonal and interannual contributions of environmental factors on isoprene and monoterpene emissions estimates over eastern Texas, Atmos. Environ., 106, 120–128, https://doi.org/10.1016/j.atmosenv.2015.01.072, 2015.

Jiang, X., Guenther, A., Potosnak, M., Geron, C., Seco, R., Karl, T., Kim, S., Gu, L., and Pallardy, S.: Isoprene emission response to drought and the impact on global atmospheric chemistry, Atmos. Environ., 183, 69–83, https://doi.org/10.1016/j.atmosenv.2018.01.026, 2018.

Kaiser, J., Jacob, D. J., Zhu, L., Travis, K. R., Fisher, J. A., González Abad, G., Zhang, L., Zhang, X., Fried, A., Crounse, J. D., St. Clair, J. M., and Wisthaler, A.: High-resolution inversion of OMI formaldehyde columns to quantify isoprene emission on ecosystem-relevant scales: application to the southeast US, Atmospheric Chem. Phys., 18, 5483–5497, https://doi.org/10.5194/acp-18-5483-2018, 2018.

Kogan, F. N.: Droughts of the Late 1980s in the United States as Derived from NOAA Polar-Orbiting Satellite Data, Bull. Am. Meteorol. Soc., 76, 655–668, https://doi.org/10.1175/1520-0477(1995)076<0655:DOTLIT>2.0.CO;2, 1995.

Kravitz, B., Guenther, A. B., Gu, L., Karl, T., Kaser, L., Pallardy, S. G., Peñuelas, J., Potosnak, M. J., and Seco, R.: A new paradigm of quantifying ecosystem stress through chemical signatures, Ecosphere, 7, e01559, https://doi.org/10.1002/ecs2.1559, 2016.

Lam, J. C. Y., Tai, A. P. K., Ducker, J. A., and Holmes, C. D.: Development of an ecophysiology module in the GEOS-Chem chemical transport model version 12.2.0 to represent biosphere-atmosphere fluxes relevant for ozone air quality, EGUsphere, 1–32, https://doi.org/10.5194/egusphere-2022-786, 2022.

692 Lei, Y., Yue, X., Liao, H., Zhang, L., Zhou, H., Tian, C., Gong, C., Ma, Y., Cao, Y., Seco, R., Karl, T., and
693 Potosnak, M.: Global Perspective of Drought Impacts on Ozone Pollution Episodes, Environ. Sci. Technol., 56,
694 3932–3940, https://doi.org/10.1021/acs.est.1c07260, 2022.

695 Li, W., Wang, Y., Flynn, J., Griffin, R. J., Guo, F., and Schnell, J. L.: Spatial Variation of Surface O3 Responses to
696 Drought Over the Contiguous United States During Summertime: Role of Precursor Emissions and Ozone
697 Chemistry, J. Geophys. Res. Atmospheres, 127, e2021JD035607, https://doi.org/10.1029/2021JD035607, 2022.

698 Liao, J., Wolfe, G. M., Hannun, R. A., St. Clair, J. M., Hanisco, T. F., Gilman, J. B., Lamplugh, A., Selimovic, V.,
699 Diskin, G. S., Nowak, J. B., Halliday, H. S., DiGangi, J. P., Hall, S. R., Ullmann, K., Holmes, C. D., Fite, C. H.,
700 Agastra, A., Ryerson, T. B., Peischl, J., Bourgeois, I., Warneke, C., Coggon, M. M., Gkatzelis, G. I., Sekimoto, K.,
701 Fried, A., Richter, D., Weibring, P., Apel, E. C., Hornbrook, R. S., Brown, S. S., Womack, C. C., Robinson, M. A.,
702 Washenfelder, R. A., Veres, P. R., and Neuman, J. A.: Formaldehyde evolution in US wildfire plumes during the
703 Fire Influence on Regional to Global Environments and Air Quality experiment (FIREX-AQ), Atmospheric Chem.
704 Phys., 21, 18319–18331, https://doi.org/10.5194/acp-21-18319-2021, 2021.

705 Lin, J.-T., Youn, D., Liang, X.-Z., and Wuebbles, D. J.: Global model simulation of summertime U.S. ozone diurnal
706 cycle and its sensitivity to PBL mixing, spatial resolution, and emissions, Atmos. Environ., 42, 8470–8483,
707 https://doi.org/10.1016/j.atmosenv.2008.08.012, 2008.

708 Marais, E. A., Jacob, D. J., Jimenez, J. L., Campuzano-Jost, P., Day, D. A., Hu, W., Krechmer, J., Zhu, L., Kim, P.
709 S., Miller, C. C., Fisher, J. A., Travis, K., Yu, K., Hanisco, T. F., Wolfe, G. M., Arkinson, H. L., Pye, H. O. T.,
710 Froyd, K. D., Liao, J., and McNeill, V. F.: Aqueous-phase mechanism for secondary organic aerosol formation from
711 isoprene: application to the southeast United States and co-benefit of SO₂ emission controls, Atmospheric Chem.
712 Phys., 16, 1603–1618, https://doi.org/10.5194/acp-16-1603-2016, 2016.

713 McKee, T. B., Doesken, N. J., and Kleist, J.: The relationship of drought frequency and duration to time scales, in:
714 Proceedings of the 8th Conference on Applied Climatology, 179–183, 1993.

715 Millet, D. B., Jacob, D. J., Turquety, S., Hudman, R. C., Wu, S., Fried, A., Walega, J., Heikes, B. G., Blake, D. R.,
716 Singh, H. B., Anderson, B. E., and Clarke, A. D.: Formaldehyde distribution over North America: Implications for
717 satellite retrievals of formaldehyde columns and isoprene emission, J. Geophys. Res. Atmospheres, 111,
718 https://doi.org/10.1029/2005JD006853, 2006.

719 Miralles, D. G., Teuling, A. J., van Heerwaarden, C. C., and Vilà-Guerau de Arellano, J.: Mega-heatwave
720 temperatures due to combined soil desiccation and atmospheric heat accumulation, Nat. Geosci., 7, 345–349,
721 https://doi.org/10.1038/ngeo2141, 2014.

722 Naimark, J. G., Fiore, A. M., Jin, X., Wang, Y., Klovenski, E., and Braneon, C.: Evaluating Drought Responses of
723 Surface Ozone Precursor Proxies: Variations With Land Cover Type, Precipitation, and Temperature, Geophys. Res.
724 Lett., 48, e2020GL091520, https://doi.org/10.1029/2020GL091520, 2021.

725 Opacka, B., Müller, J.-F., Stavrakou, T., Miralles, D. G., Koppa, A., Pagán, B. R., Potosnak, M. J., Seco, R., De
726 Smedt, I., and Guenther, A. B.: Impact of Drought on Isoprene Fluxes Assessed Using Field Data, Satellite-Based
727 GLEAM Soil Moisture and HCHO Observations from OMI, Remote Sens., 14, 2021,
728 https://doi.org/10.3390/rs14092021, 2022.

729 Otu-Larbi, F., Bolas, C. G., Ferracci, V., Staniaszek, Z., Jones, R. L., Malhi, Y., Harris, N. R. P., Wild, O., and
730 Ashworth, K.: Modelling the effect of the 2018 summer heatwave and drought on isoprene emissions in a UK
731 woodland, Glob. Change Biol., 26, 2320–2335, https://doi.org/10.1111/gcb.14963, 2020.

732 Pacifico, F., Harrison, S. P., Jones, C. D., and Sitch, S.: Isoprene emissions and climate, Atmos. Environ., 43, 6121–
733 6135, https://doi.org/10.1016/j.atmosenv.2009.09.002, 2009.

Palmer, P. I., Jacob, D. J., Fiore, A. M., Martin, R. V., Chance, K., and Kurosu, T. P.: Mapping isoprene emissions over North America using formaldehyde column observations from space, J. Geophys. Res. Atmospheres, 108, https://doi.org/10.1029/2002JD002153, 2003.

Palmer, W. C.: Meteorological Drought, U.S. Department of Commerce, Weather Bureau, 68 pp., 1965.

Potosnak, M. J., LeStourgeon, L., Pallardy, S. G., Hosman, K. P., Gu, L., Karl, T., Geron, C., and Guenther, A. B.: Observed and modeled ecosystem isoprene fluxes from an oak-dominated temperate forest and the influence of drought stress, Atmos. Environ., 84, 314–322, https://doi.org/10.1016/j.atmosenv.2013.11.055, 2014.

Pye, H. O. T., Chan, A. W. H., Barkley, M. P., and Seinfeld, J. H.: Global modeling of organic aerosol: the importance of reactive nitrogen (NO_x and NO_3), Atmospheric Chem. Phys., 10, 11261–11276, https://doi.org/10.5194/acp-10-11261-2010, 2010.

Pye, H. O. T., Murphy, B. N., Xu, L., Ng, N. L., Carlton, A. G., Guo, H., Weber, R., Vasilakos, P., Appel, K. W., Budisulistiorini, S. H., Surratt, J. D., Nenes, A., Hu, W., Jimenez, J. L., Isaacman-VanWertz, G., Misztal, P. K., and Goldstein, A. H.: On the implications of aerosol liquid water and phase separation for organic aerosol mass, Atmospheric Chem. Phys., 17, 343–369, https://doi.org/10.5194/acp-17-343-2017, 2017.

Schnell, J. L., Holmes, C. D., Jangam, A., and Prather, M. J.: Skill in forecasting extreme ozone pollution episodes with a global atmospheric chemistry model, Atmospheric Chem. Phys., 14, 7721–7739, https://doi.org/10.5194/acp-14-7721-2014, 2014.

Schroder, J. C., Campuzano-Jost, P., Day, D. A., Shah, V., Larson, K., Sommers, J. M., Sullivan, A. P., Campos, T., Reeves, J. M., Hills, A., Hornbrook, R. S., Blake, N. J., Scheuer, E., Guo, H., Fibiger, D. L., McDuffie, E. E., Hayes, P. L., Weber, R. J., Dibb, J. E., Apel, E. C., Jaeglé, L., Brown, S. S., Thornton, J. A., and Jimenez, J. L.: Sources and Secondary Production of Organic Aerosols in the Northeastern United States during WINTER, J. Geophys. Res. Atmospheres, 123, 7771–7796, https://doi.org/10.1029/2018JD028475, 2018.

Seager, R., Tzanova, A., and Nakamura, J.: Drought in the Southeastern United States: Causes, Variability over the Last Millennium, and the Potential for Future Hydroclimate Change, J. Clim., 22, 5021–5045, https://doi.org/10.1175/2009JCLI2683.1, 2009.

Seco, R., Karl, T., Guenther, A., Hosman, K. P., Pallardy, S. G., Gu, L., Geron, C., Harley, P., and Kim, S.: Ecosystem-scale volatile organic compound fluxes during an extreme drought in a broadleaf temperate forest of the Missouri Ozarks (central USA), Glob. Change Biol., 21, 3657–3674, https://doi.org/10.1111/gcb.12980, 2015.

Seco, R., Holst, T., Davie-Martin, C. L., Simin, T., Guenther, A., Pirk, N., Rinne, J., and Rinnan, R.: Strong isoprene emission response to temperature in tundra vegetation, Proc. Natl. Acad. Sci., 119, e2118014119, https://doi.org/10.1073/pnas.2118014119, 2022.

Shen, L., Jacob, D. J., Zhu, L., Zhang, Q., Zheng, B., Sulprizio, M. P., Li, K., De Smedt, I., González Abad, G., Cao, H., Fu, T.-M., and Liao, H.: The 2005–2016 Trends of Formaldehyde Columns Over China Observed by Satellites: Increasing Anthropogenic Emissions of Volatile Organic Compounds and Decreasing Agricultural Fire Emissions, Geophys. Res. Lett., 46, 4468–4475, https://doi.org/10.1029/2019GL082172, 2019.

Sindelarova, K., Granier, C., Bouarar, I., Guenther, A., Tilmes, S., Stavrakou, T., Müller, J.-F., Kuhn, U., Stefani, P., and Knorr, W.: Global data set of biogenic VOC emissions calculated by the MEGAN model over the last 30 years, Atmospheric Chem. Phys., 14, 9317–9341, https://doi.org/10.5194/acp-14-9317-2014, 2014.

Sprengnether, M., Demerjian, K. L., Donahue, N. M., and Anderson, J. G.: Product analysis of the OH oxidation of isoprene and 1,3-butadiene in the presence of NO, J. Geophys. Res. Atmospheres, 107, ACH 8-1-ACH 8-13, https://doi.org/10.1029/2001JD000716, 2002.

775 Squire, O. J., Archibald, A. T., Griffiths, P. T., Jenkin, M. E., Smith, D., and Pyle, J. A.: Influence of isoprene
776 chemical mechanism on modelled changes in tropospheric ozone due to climate and land use over the 21st century,
777 Atmospheric Chem. Phys., 15, 5123–5143, https://doi.org/10.5194/acp-15-5123-2015, 2015.

778 Stavrakou, T., Müller, J.-F., Bauwens, M., De Smedt, I., Van Roozendael, M., and Guenther, A.: Impact of Short-
779 Term Climate Variability on Volatile Organic Compounds Emissions Assessed Using OMI Satellite Formaldehyde
780 Observations, Geophys. Res. Lett., 45, 8681–8689, https://doi.org/10.1029/2018GL078676, 2018.

781 Svoboda, M., LeComte, D., Hayes, M., Heim, R., Gleason, K., Angel, J., Rippey, B., Tinker, R., Palecki, M.,
782 Stooksbury, D., Miskus, D., and Stephens, S.: THE DROUGHT MONITOR, Bull. Am. Meteorol. Soc., 83, 1181–
783 1190, https://doi.org/10.1175/1520-0477-83.8.1181, 2002.

784 Svoboda, M. D., Fuchs, B. A., Poulsen, C. C., and Nothwehr, J. R.: The drought risk atlas: Enhancing decision
785 support for drought risk management in the United States, J. Hydrol., 526, 274–286,
786 https://doi.org/10.1016/j.jhydrol.2015.01.006, 2015.

787 Travis, K. R. and Jacob, D. J.: Systematic bias in evaluating chemical transport models with maximum daily
788 8 h average (MDA8) surface ozone for air quality applications: a case study with GEOS-Chem v9.02,
789 Geosci. Model Dev., 12, 3641–3648, https://doi.org/10.5194/gmd-12-3641-2019, 2019.

790 Travis, K. R., Jacob, D. J., Fisher, J. A., Kim, P. S., Marais, E. A., Zhu, L., Yu, K., Miller, C. C., Yantosca, R. M.,
791 Sulprizio, M. P., Thompson, A. M., Wennberg, P. O., Crounse, J. D., St. Clair, J. M., Cohen, R. C., Laughner, J. L.,
792 Dibb, J. E., Hall, S. R., Ullmann, K., Wolfe, G. M., Pollack, I. B., Peischl, J., Neuman, J. A., and Zhou, X.: Why do
793 models overestimate surface ozone in the Southeast United States?, Atmospheric Chem. Phys., 16, 13561–13577,
794 https://doi.org/10.5194/acp-16-13561-2016, 2016.

795 Trenberth, K. E., Dai, A., van der Schrier, G., Jones, P. D., Barichivich, J., Briffa, K. R., and Sheffield, J.: Global
796 warming and changes in drought, Nat. Clim. Change, 4, 17–22, https://doi.org/10.1038/nclimate2067, 2014.

797 Trugman, A. T., Medvigy, D., Mankin, J. S., and Anderegg, W. R. L.: Soil Moisture Stress as a Major Driver of
798 Carbon Cycle Uncertainty, Geophys. Res. Lett., 45, 6495–6503, https://doi.org/10.1029/2018GL078131, 2018.

799 Vicente-Serrano, S. M., Beguería, S., and López-Moreno, J. I.: A Multiscalar Drought Index Sensitive to Global
800 Warming: The Standardized Precipitation Evapotranspiration Index, J. Clim., 23, 1696–1718,
801 https://doi.org/10.1175/2009JCLI2909.1, 2010.

802 Wang, Y., Xie, Y., Dong, W., Ming, Y., Wang, J., and Shen, L.: Adverse effects of increasing drought on air quality
803 via natural processes, Atmospheric Chem. Phys., 17, 12827–12843, https://doi.org/10.5194/acp-17-12827-2017,
804 2017.

805 Wells, K. C., Millet, D. B., Payne, V. H., Deventer, M. J., Bates, K. H., de Gouw, J. A., Graus, M., Warneke, C.,
806 Wisthaler, A., and Fuentes, J. D.: Satellite isoprene retrievals constrain emissions and atmospheric oxidation,
807 Nature, 585, 225–233, https://doi.org/10.1038/s41586-020-2664-3, 2020.

808 Willeke, G., Hosking, J. R. M., Wallis, J. R., and Guttman, N. B.: The national drought atlas, Inst. Water Resour.
809 Rep., 94, 1994.

810 Xu, L., Guo, H., Boyd, C. M., Klein, M., Bougiatioti, A., Cerully, K. M., Hite, J. R., Isaacman-VanWertz, G.,
811 Kreisberg, N. M., and Knote, C.: Effects of anthropogenic emissions on aerosol formation from isoprene and
812 monoterpenes in the southeastern United States, Proc. Natl. Acad. Sci., 112, 37–42, 2015.

813 Yuan, H., Dai, Y., Xiao, Z., Ji, D., and Shangguan, W.: Reprocessing the MODIS Leaf Area Index products for land
814 surface and climate modelling, Remote Sens. Environ., 115, 1171–1187, https://doi.org/10.1016/j.rse.2011.01.001,
815 2011.

816   Zhao, T., Mao, J., Simpson, W. R., De Smedt, I., Zhu, L., Hanisco, T. F., Wolfe, G. M., St. Clair, J. M., González
817   Abad, G., Nowlan, C. R., Barletta, B., Meinardi, S., Blake, D. R., Apel, E. C., and Hornbrook, R. S.: Source and
818   variability of formaldehyde (HCHO) at northern high latitudes: an integrated satellite, aircraft, and model study,
819   Atmospheric Chem. Phys., 22, 7163–7178, https://doi.org/10.5194/acp-22-7163-2022, 2022.

820   Zheng, Y., Unger, N., Tadić, J. M., Seco, R., Guenther, A. B., Barkley, M. P., Potosnak, M. J., Murray, L. T.,
821   Michalak, A. M., Qiu, X., Kim, S., Karl, T., Gu, L., and Pallardy, S. G.: Drought impacts on photosynthesis,
822   isoprene emission and atmospheric formaldehyde in a mid-latitude forest, Atmos. Environ., 167, 190–201,
823   https://doi.org/10.1016/j.atmosenv.2017.08.017, 2017.

824   Zheng, Y., Thornton, J. A., Ng, N. L., Cao, H., Henze, D. K., McDuffie, E. E., Hu, W., Jimenez, J. L., Marais, E. A.,
825   Edgerton, E., and Mao, J.: Long-term observational constraints of organic aerosol dependence on inorganic species
826   in the southeast US, Atmospheric Chem. Phys., 20, 13091–13107, https://doi.org/10.5194/acp-20-13091-2020,
827   2020.

828   Zhu, L., Jacob, D. J., Kim, P. S., Fisher, J. A., Yu, K., Travis, K. R., Mickley, L. J., Yantosca, R. M., Sulprizio, M.
829   P., De Smedt, I., González Abad, G., Chance, K., Li, C., Ferrare, R., Fried, A., Hair, J. W., Hanisco, T. F., Richter,
830   D., Jo Scarino, A., Walega, J., Weibring, P., and Wolfe, G. M.: Observing atmospheric formaldehyde (HCHO) from
831   space: validation and intercomparison of six retrievals from four satellites (OMI, GOME2A, GOME2B, OMPS)
832   with SEAC[4]RS aircraft observations over the southeast US, Atmospheric Chem. Phys., 16, 13477–13490,
833   https://doi.org/10.5194/acp-16-13477-2016, 2016.

834